Patchiness of plankton communities at fronts explained by Lagrangian history of upwelled water parcels

Shailja Gangrade

sgangrad@ucsd.edu

Scripps Institution of Oceanography, University of California San Diego, La Jolla, California, USA

Inès Mangolte

Institut de Recherche pour le Développement https://orcid.org/0000-0002-0358-844X

Research Article

Keywords: plankton, patchiness, convergence, front, Lagrangian, backtracking, upwelling, ecology, transport

Posted Date: April 12th, 2024

DOI: https://doi.org/10.21203/rs.3.rs-4250467/v1

Additional Declarations: The authors declare no competing interests.

Patchiness of plankton communities at fronts explained by Lagrangian history of upwelled water parcels

Shailja Gangrade[1*] and Inès Mangolte[2,3]

[1]Scripps Institution of Oceanography, University of California San Diego, La Jolla, California, USA

[2]LOCEAN (Laboratoire d'Océanographie et du Climat), Institut Pierre Simon Laplace (Sorbonne Université/CNRS/IRD/MNHN), Paris, France

[3]ENTROPIE, IRD/Université de la Réunion/Université de Nouvelle-Calédonie/CNRS/Ifremer, Noumea, New Caledonia

[*]Corresponding author: Shailja Gangrade, sgangrad@ucsd.edu

Running Head: Lagrangian history explains plankton patchiness

Significance Statement

This study refines our view of biological patchiness at ocean fronts. Commonly, enhanced biomass or biological variability at and across fronts has been attributed to local processes that inject nutrients into the euphotic zone, stimulating phytoplankton growth and subsequent secondary production. However, we challenge this two-dimensional perspective and, through our combined in-situ and satellite-data approach, show that frontal plankton community structure is actually best explained by tracing water parcels to their origins and understanding them in the context of their spatial and temporal histories. We therefore advance our knowledge of physical-biological dynamics at these ecological hotspots and describe a novel framework, the Lagrangian history, that can be applied to observational data. We also demonstrate that, while several other studies have adopted similar approaches through modeling or forward-tracking of in situ data, a backtracking, data-driven approach is robust.

Our study presents a novel framework that a wide variety of ocean – and aquatic – scientists can apply and build upon. By describing our hypothesis-driven approach that incorporates publicly available observational data from a long-term monitoring site in a novel way, our aim is to advance scientific understanding of complex ocean systems, such as fronts. Therefore, we find our study is optimally suited for L&O and hope for it to reach a broad aquatic science audience.

Author Contribution

Shailja Gangrade: Conceptualization (equal); Data curation (equal); Formal analysis (lead); Methodology (equal); Software (lead); Visualization (lead); Writing – Original Draft Preparation (equal); Writing – Review & Editing (equal). **Inès Mangolte**: Conceptualization (equal); Data curation (equal); Formal analysis (supporting); Software (supporting); Visualization (supporting); Methodology (equal); Writing – Original Draft Preparation (equal); Writing – Review & Editing (equal).

Abstract

The transport of plankton by highly dynamic (sub)mesoscale currents—often associated with fronts and eddies—shapes the structure of plankton communities on the same time scales as biotic processes, such as growth and predation. The resulting bio-physical couplings generate heterogeneities in their finescale distributions (1-10 km), or "patchiness." Here, we test the hypothesis that cross-frontal plankton patchiness at a front found 200-250 km offshore in the California Current System was influenced by wind-driven upwelling conditions upstream of the front. We show that *in situ* Eulerian measurements (cross-frontal transects) can be interpreted in a Lagrangian framework by using satellite-derived current velocities to trace water parcels backward in time to their coastal origins. We find that the majority of the water parcels sampled at this front originated along the central California coast during different episodic wind-driven upwelling pulses and followed various trajectories before converging temporarily at the front. In response to nutrient injections at the coast, plankton communities transformed during their journeys from the coast to the sampling zone, with a succession of phytoplankton and zooplankton blooms. The cross-frontal sampling captured the convergence of these distinct water parcels at different points in their biological histories, which resulted in the observed spatial patchiness. Our results suggest that identifying the processes controlling frontal plankton communities requires understanding them in the context of their spatial and temporal histories, rather than as two-dimensional responses to local frontal processes. In particular, Lagrangian approaches should be more widely applied to understand critical ecological patterns in highly dynamic systems.

Introduction

Marine plankton are passively drifting organisms of immense ecological and biogeochemical importance in the functioning of ocean ecosystems. Plankton spatial distributions are profoundly impacted by ocean currents, particularly in regions of highly energetic mesoscale stirring. In stirring features, such as fronts and eddies, horizontal current velocities can reach up to 50-80 km/day (McWilliams, 2016; Barth et al., 2000; Kosro and Huyer, 1986; Zaba et al., 2021), resulting in transport over long distances within a few days to weeks. Importantly, biological processes, such as growth, competition, or predation, occur on similar time scales. Phytoplankton blooms, for instance, usually develop within a few days (Lewandowska et al., 2015), and most mesozooplankton can complete a reproduction cycle in a few weeks (Kotori, 1999; Cohen and Morin, 1990; Deibel and Lowen, 2012; Bouquet et al., 2018; Eiane and Ohman, 2004).

As a result, physical and biological processes are highly coupled, often resulting in a high level of heterogeneity in biological properties on small spatial scales (1-10 km), or "patchiness." Disentangling the interacting roles of physics and biology in driving plankton patchiness has been a central question in ecology for many decades (Levin and Segel, 1976; Gower et al., 1980; Abraham, 1998; Martin, 2003; McGillicuddy and Franks, 2019). The processes driving plankton diversity and community structure have similarly been examined, with many studies showing the influence of bottom-up and top-down trophic interactions (Allen et al., 2005; Mangolte et al., 2022; Dugenne et al., 2020), transport (Wilkins et al., 2013), or a combination of all of these processes (Clayton et al., 2013; Lévy et al., 2014; Schmid et al., 2023). Lagrangian studies have also explored how water parcels are connected between remote regions (i.e., their "connectivity") across differing spatial scales–from a single basin to the global ocean–and how this connectivity influences various biological processes, such as genetic similarity or larval dispersal (Rossi et al., 2014; Wilkins et al., 2013; Jönsson and Watson, 2016).

Recently, many studies have employed Lagrangian approaches to describe how plankton communi-

ties transform as they are transported, sometimes hundreds of kilometers in a matter of days (Lehahn et al., 2017, 2018; Messié and Chavez, 2017; Messié et al., 2022). These approaches have shown that the abundance of plankton is not only determined by their immediate environment (e.g., temperature and nutrient concentration (Mousing et al., 2016; Tzortzis et al., 2021; Haberlin et al., 2019)) but is also shaped by the conditions experienced during the previous weeks at different locations (D'Ovidio et al., 2010, 2015; Hernández-Carrasco et al., 2023; Gangrade and Franks, 2023). The first view–local environmental conditions determine species abundance–can be likened to the classic Eulerian concept of an "ecological niche." This concept was originally developed for terrestrial ecosystems and successfully applied to the ocean on large scales (e.g., biogeochemical provinces as in Longhurst (2006) and Beaugrand et al. (2019)). The second view–transport history shapes species distributions–is a Lagrangian concept, relevant to small scales and specific to passively drifting marine plankton. This concept has been described as "fluid dynamical niches" (D'Ovidio et al., 2010): finescale plankton patchiness is a moving mosaic of water parcels carrying different plankton communities.

Here, we investigate the processes generating finescale cross-frontal patchiness in plankton community structure in an Eastern Boundary Upwelling System (EBUS). In EBUSs such as the California Current System (CCS), wind-driven vertical nutrient injections at the coast modulate biological variability at time scales ranging from days to decades (Jacox et al., 2018; Messié et al., 2023), while horizontal currents structure the ecosystem spatially by advecting recently upwelled waters in filaments from the coast to offshore (Chelton et al., 2011; Renault et al., 2021; Mauzole et al., 2020; Zaba et al., 2021; Bourne et al., 2021). The CCS is thus structured by a cross-shore gradient: new production (primary production resulting from nutrient inputs from outside the euphotic zone, such as coastal upwelling) generally takes place inshore while export takes place further offshore (Plattner et al., 2005; Stukel et al., 2013; Chabert et al., 2021). In addition to the small-scale circulation (filaments and eddies), the CCS is composed of two main flow features: the California Current

(CC), an equatorward-flowing current of subarctic origin; and, the California Undercurrent (CU), a subsurface poleward-flowing current of equatorial origin (Lynn and Simpson, 1987; Huyer et al., 1991; Bograd et al., 2015, 2019).

We use the case study of a front in the southern CCS, characterized by an intense frontal jet and horizontally converging flow (de Verneil et al., 2019), to explore how coastal upwelling pulses propagate offshore (Gangrade and Franks, 2023) and generate plankton patchiness (Mangolte et al., 2023) on time scales of a few weeks. We evaluate the relationship between plankton distributions and the characteristics of water parcels based on two different frameworks. First, we describe the water parcels by their *in situ* hydrographic properties (the *regional water-mass types* derived from temperature and salinity: CC or CU). Second, we describe the water parcels based on their Lagrangian trajectories since upwelling (the *water-mass history*, derived from a backtracking analysis). Our results show that both frameworks give insights into the drivers of plankton community structure; however, the Lagrangian method provides a more detailed understanding of the mechanisms generating local finescale patchiness.

Data and Methods

Cruise data

Biological and hydrographic measurements were collected during the California Current Ecosystem Long-Term Ecological Research (CCE LTER) Process Cruise P1208 in August 2012. This cruise sampled an eddy-associated front, dubbed "E-Front," located approximately 200-250 km offshore of Point Conception, California. This front was positioned between an anticyclonic eddy to the west (offshore) and a cyclonic eddy to the east (inshore) (De Verneil and Franks, 2015; Stukel et al., 2017; Bednaršek and Ohman, 2015; Gangrade and Franks, 2023). The cross-frontal sampling included 2 transects (E1 and E2) with high horizontal resolution (3-5 km between consecutive stations), conducted on 4-5 August 2012 and 20-21 August 2012 respectively (Figure 1).

At each transect station, a CTD (conductivity, temperature, depth) vertical profile was recorded

down to 350 m and binned to 1-m vertical resolution, and water samples were collected in Niskin bottles at discrete depths (5-6 levels between 0 and 100 m) on the ascent. The CTD rosette included a fluorometer which measured *in vivo* chlorophyll-*a* fluorescence. After the CTD cast, zooplankton samples were collected with a 0.71-m diameter, 202-μm mesh vertical Bongo net tow from 0 to 100 m. The plankton samples were later analyzed using three different methods; the full dataset was described in detail in Mangolte et al. (2023) (see their Figure 2) and is summarized here (Supporting Information Table S1). Flow cytometry was performed on the Niskin bottle water samples (0-100 m), producing the abundance (number of cells/L) of 4 taxa of pico-plankton (< 2 μm) identified by their light-scattering properties. High-performance liquid chromatography (HPLC) was performed on the surface Niskin bottle samples; the concentrations of chlorophyll *a* and accessory pigments were measured and used to determine the contributions (percentage) of 8 phytoplankton taxa relative to the total chlorophyll (Goericke and Montoya, 1998). Zooplankton samples, collected from vertical Bongo nets, were preserved in 1.8% buffered formaldehyde, and organisms were then identified in the lab using the ZooScan semi-automated imaging system (Gorsky et al., 2010; Ohman et al., 2012) with 100% manual validation, producing the vertically integrated abundance (number of organisms m^{-2}) of 15 groups of mesozooplankton.

Water-mass classification

To describe the distributions of California Current (CC) and California Undercurrent (CU) waters across E-Front, we classified the water sampled by the CTD at each vertical level as CC or CU based on temperature, salinity, and distance-from-shore criteria defined by Zaba et al. (2021) (Supporting Information Figure S1). At the boundary between CC and CU, small-scale three-dimensional mixing resulted in waters with intermediate temperature-salinity signatures that were neither CC nor CU; we classified those waters as a third water-mass type: MIX.

Statistical analysis of water-mass type and abundance association

We combined the information on hydrographic classifications (CC, CU, or MIX) and plankton abundances to determine whether plankton were preferentially associated with a certain water mass. For phytoplankton and bacteria, we used abundances and water-mass type classification at each Niskin bottle depth. Because the Bongo nets generate vertically integrated zooplankton abundances, we found it most informative to relate the zooplankton distributions to the dominant water-mass type in the sampled water column (0-100 m). We defined this dominant water type as CC or CU if more than 50% of the vertical bins were classified as such, and MIX in other cases. The abundances in each water type were first examined qualitatively (Supporting Information Figures S2-S5) and Kruskal-Wallis tests were then used to determine whether abundances among the three water-mass types were statistically different.

Water-parcel tracking

Using satellite-derived velocity fields, we tracked the water parcels of each transect station backward in time from the time of sampling for approximately 2 months (66 days) using the Euler method, described in Gangrade and Franks (2023). Horizontal velocity products were obtained from the Copernicus Marine Environment Monitoring Service (CMEMS; https://doi.org/10.48670/mds-00327). The zonal and meridional velocities are provided with a 1-day temporal resolution and a 0.25-degree horizontal resolution. The velocities include a geostrophic component (derived from satellite altimeter measurements) and a wind-driven Ekman component at 0 m and 15 m depth, derived from the wind stress from the ERA reanalysis (Rio et al., 2014). We selected the geostrophic plus 15-m Ekman velocities for our tracking analysis because they are more representative of the velocities impacting the distribution of planktonic organisms in the euphotic layer. It should be noted that we limited the backtracking to 2 months to minimize the contribution of stirring and mixing to water-mass property changes.

Random parcel seeding

To estimate the uncertainty associated with these trajectories (primarily caused by the coarse 0.25-degree spatial resolution of the velocities), we performed the backtracking for 100 parcels seeded randomly within a 0.0625°(approximately 5 km) radius around each transect station. We then described the presumed upwelling conditions experienced by the waters sampled at each station based on this ensemble of possible trajectories.

Upwelling pulses

Wind-driven upwelling pulses were determined from the Coastal Upwelling Transport Index (CUTI; Jacox et al. 2018), which is defined in 1° latitudinal bands. We defined anomalies relative to the temporal average of the CUTI during the study period (June to August 2012). Upwelling pulses were defined as short periods (typically a few days) of positive CUTI anomalies. Large positive anomaly values indicate strong upwelling pulses that are expected to upwell high-nutrient waters from below the euphotic zone and generate a strong biological response.

Upwelling conditions upstream of the front

We used the backward-in-time trajectories and CUTI values along the California coast to determine how many days before being sampled at the front a water parcel had experienced an upwelling pulse, and the intensity of that pulse. First, we determined whether each sampled water parcel was in the coastal region influenced by wind-driven upwelling (i.e., within 25 km of the coastline; Huyer 1983) in the two months before sampling. Next, for parcels with coastal origins, we determined whether the parcel experienced an upwelling pulse. If it did, we recorded the location (latitude, longitude, and date) of the water parcel when it was last at the coast during an upwelling pulse; these coordinates thus represented the parcel's temporal and spatial origin. Finally, we characterized a parcel's upwelling pulse using two criteria: (1) the intensity of the upwelling pulse (CUTI anomaly) at the parcel's origin, and (2) the water parcel age since the upwelling pulse (i.e., the time elapsed

between the origin date and the frontal sampling date, in days). We followed this procedure for all 100 points seeded around each transect station.

Results

Distribution of water masses and chlorophyll *a* across the front

In the upper 100 m, the eastern (inshore) side of the front was composed of primarily CU waters while the western (offshore) side was composed of primarily CC waters (Figure 2). The interface between the water masses, where water-mass mixing occurred, was composed of a 2-15 km wide layer of MIX waters. While this MIX layer persisted for at least the duration of the cruise (approximately 1 month), its geometry changed between the two transects, which were sampled two weeks apart. During the first transect (E1, Figure 2a), the MIX water layer between the CC and CU water masses was tilted across the front, with CU waters extending offshore below the CC waters (and vice versa: CC waters extending inshore above CU waters). During the second transect (E2, Figure 2b), the MIX layer was mostly vertical, with the exception of an intrusion of offshore CC waters into inshore CU waters below the surface (30-70 m).

The distribution of Chl-a fluorescence (Figure 2, hatched contours) across the front was closely related to the distribution of the water masses. Generally, CC waters contained less Chl-a than CU waters. Most strikingly, small patches of high Chl-a were associated with MIX waters at the interface between CC and CU waters. This visual pattern was then confirmed by the results of a Kruskal-Wallis statistical test summarized in Table 1, where statistically significant associations are indicated by "X", and taxa with a weak association with a water mass (identified qualitatively, but without passing the Kruskal-Wallis tests) with "x." The geometry of the Chl-a patches was closely aligned with the boundaries between the water masses, consistent with a coupling of hydrographic and biological properties. In the next section, we investigate this coupling in more detail by looking at the individual phytoplankton and zooplankton taxa.

Distribution of plankton taxa across the front

We analyzed the spatial distribution of 23 plankton taxa (including bacteria, phytoplankton and zooplankton) across the front to characterize their relationship with water-mass type. We found that spatial distribution across the front varied by taxon; bacteria, phytoplankton, and zooplankton were not necessarily co-located in space in terms of abundance (Figure 3). This cross-frontal patchiness and variability both within and across transects prompted us to investigate the association of each taxon with water-mass type.

We considered that a given taxon was consistently associated with CC or CU if it had a significantly higher abundance in that water-mass type for the two transects conducted two weeks apart during the cruise. We found that 8 taxa (chlorophytes, cryptophytes, dinoflagellates, pelagophytes, prymnesiophytes, heterotrophic bacteria, rhizaria, and pteropods) were consistently associated with CU waters, and 1 taxon (*Prochlorococcus*) was consistently associated with CC waters in both transects (Table 1, upper rows).

The remaining taxa (n=14) did not have a consistent association with a single water-mass type (CC or CU) and displayed a range of patterns (Table 1, bottom rows). Ostracods were associated with MIX waters in both transects, while the 13 other taxa exhibited time-dependent water-mass associations. Doliolids were associated with CU waters in E1, but CC waters in E2; three copepod taxa, polychaetes, euphausiids, and other crustaceans were associated with MIX waters in E1, but with CU waters in E2. The remaining taxa were associated with a particular water mass in only one transect, with no statistically significant association in the other: pico-eukaryotes, *Synechococcus*, chaetognaths, cnidarians, and appendicularians were associated with MIX waters in E1 only; diatoms were associated with MIX waters in E2 only (Supporting Information Table S2 and Table S3). While the distributions of some plankton taxa were explained by the local water mass type (consistent association with either CC or CU), the majority were not. In the next sections, we explore the possibility that the water-mass history (through a Lagrangian approach) could provide an alternative

explanation.

Horizontal convergence of water masses at the front

Here, we examine the origins of the water parcels sampled across the front to investigate how wind-driven coastal upwelling upstream of the front drove temporal and spatial biological variability across the front.

Geographic origins

Our backward-in-time tracking showed that waters sampled during both E1 and E2 had variable geographic origins (Figure 4). While almost all the stations contained waters that originated at the coast in the two months before sampling (Supporting Information Table S4), the origin locations varied. Waters sampled in E1 originated from a broad stretch of the coast (from 34°N to 39°N, about 500 km), while the waters sampled in E2 originated in a narrower region (34°N to 36°N, about 200 km). Thus, for both transects, water parcels sampled within 25 km of each other at the front were hundreds of kilometers apart two months earlier. The lengths and geometries of parcel trajectories from the coast to the transect locations were also variable: water parcels sampled on the offshore side of the transects generally had long, meandering trajectories, while water parcels sampled on the inshore side of the transects generally had shorter, more direct trajectories to the front (Figure 4).

Temporal origins: upwelling pulses

Water parcels sampled at the frontal transect sites also originated at the coast at different times. For simplicity, we assumed that water parcels originating in the coastal region during an upwelling pulse were upwelled from depth. Remarkably, despite the fact that upwelling pulses only occurred 40-50% of the time (Figure 5), our backtracking analysis revealed that almost all the water parcels sampled during the cruise originated at the coast during an upwelling pulse (Supporting Information Table S4). Some of the sampled parcels were upwelled much more recently than others: the median ages (times since upwelling) ranged from 8 to 51 days for Transect E1, and from 11 to 43 days

for Transect E2 (Figure 6). For E1, the inshore stations tended to contain more recently upwelled water than the offshore stations (Figure 6a). However, counter-intuitively, for E2, the oldest waters (median age = 43 days) were found at the two most inshore stations (E2 Stations 1 and 2), while the other stations contained more recently upwelled water with median ages ranging from 11 to 15 days (Figure 6b). We discuss this apparent discrepancy further in the next section. Finally, we found that the intensities of the upwelling pulses were variable along the coast, with the CUTI anomaly ranging from approximately 0 to 1.8 $m^2 s^{-1}$ (Figures 5, 6).

Relationship between upwelling and water masses

The distributions of CC and CU waters across the front were related to their geographic and temporal origins during upwelling pulses. The data collected during the Transect E1 supported the typical scenario of subsurface nearshore CU waters being entrained first upward (into the euphotic zone by upwelling) and then offshore by transport (Zaba et al., 2018, 2021). The water parcels with short, direct trajectories between coastal upwelling sites and the transect location (E1 Stations 10-13) retained a CU temperature-salinity signature, while parcels with long, meandering, offshore trajectories (E1 Stations 1-9) mixed with CC waters, leading to their classification as MIX, and CC for the oldest water parcels (Figures 2 and 4).

Data from E2, however, indicates a more complicated scenario. E2 included recently upwelled water parcels (with very short and direct trajectories from the coast) that were classified as CC (E2 Stations 5-10). Conversely, some older water parcels with long meandering trajectories were classified as CU (E2 Stations 1-2, Figures 4 and 6). Some trajectories can be seen meandering strongly between offshore and coastal regions (Figure 4); this suggests that CC waters may have first been brought from offshore into the coastal regions and then were advected offshore again along with newly upwelled waters.

Summary: Lagrangian physics

Overall, our results indicate that water masses with entirely different histories (in terms of their geographic origins, the intensities of upwelling pulses experienced, and the geometries of their trajectories) converged at E-Front. These unique histories led to distinct water-mass signatures (CC, CU, or MIX) being sampled across the front within 25-km transects. Importantly, the trajectories depended on the regional (sub)mesoscale circulation, which is extremely variable on time scales of weeks to months.

Biological history along water-parcel trajectories

We investigated the relationship between the age of an upwelled water parcel and the plankton community found within this water parcel. We defined the "biological history" of a water parcel as the relationship between its age (defined as time since upwelling) and abundances of key planktonic taxa within that water parcel.

By combining the trajectories of water parcels of different ages, we reconstructed the biological histories of these water parcels between the upwelling pulse (at the coast) and sampling (at the transects). Since we found no relationship between plankton abundance and upwelling pulse intensity (Supporting Information Figures S6-S8), we assumed that all upwelling pulses generated a similar biological response.

We found that the abundances of diatoms and copepods exhibited the clearest relationship with age since upwelling, with peaks at about 15 days and 30 days, respectively, after a water parcel experienced an upwelling pulse (Figure 7). Interestingly, this succession is consistent with the well-known trophic dynamics of these two taxa. Diatom doubling times are only a few days in the presence of abundant nutrients, such as those provided by an upwelling pulse (Sarthou et al., 2005). Copepods, which are among the main predators of diatoms, can complete a reproduction cycle in 28 days (Eiane and Ohman, 2004). Thus, we interpreted this succession of abundance peaks as a diatom

bloom in response to the upwelling pulse, followed by a copepod bloom in response to the increase of their food supply. The other taxa showed more complex relationships between abundance and age, which, due to higher uncertainties regarding their food-web dynamics and growth rates, prevented us from deriving robust interpretations of the influence of the upwelling pulses (see Supporting Information, Biological responses of non-diatom and non-copepod taxa and Figures S6-S8).

Summary: Lagrangian biology

Here, we showed that the differences in plankton community composition between the water parcels on a cross-frontal transect were explained by differences in their histories, and more specifically, by their age since upwelling (quantified by the time elapsed since they experienced a wind-driven upwelling pulse at the coast). "Young" water parcels had high abundances of large phytoplankton (i.e., diatoms), while "older" water parcels had high abundances of herbivorous mesozooplankton (i.e., copepods).

Discussion

In this study, we sought to investigate the influence of wind-driven coastal upwelling on the finescale plankton community structure observed across a front. We first attempted to relate the ecosystem structure to the hydrographic properties of water (the water mass-type, CC or CU), relying on previous literature that established that CU waters are generally recently upwelled while CC waters are found offshore. However, we found that the explanatory power of this approach was limited: many plankton taxa were either found at the interface between the two water masses, or they did not have a consistent association with a particular water-mass type.

We then used a Lagrangian approach to describe the history of the water parcels by backtracking each parcel to its origin. Our results from this approach demonstrated a consistent story (Figure 8). Intermittent increases in alongshore wind generated short upwelling pulses every week or so, transporting deep, nutrient-rich waters into the euphotic zone in the coastal region. These water parcels

were then advected offshore, following distinct trajectories until they reached the front where they were sampled. During this advection, the plankton community carried by each water parcel transformed in response to nutrient injections, experiencing a succession of phytoplankton and zooplankton blooms. Eventually, various distinct water parcels were brought together by the horizontally convergent flow at E-Front. Because the water parcels were generated by different upwelling pulses (i.e., at different dates and locations along the coast), they contained plankton communities at different stages of maturity since upwelling (i.e., young parcels were dominated by phytoplankton, and older parcels dominated by zooplankton). However, because they converged at the front, they were located very close to one another in space (within the 25 km sampled by an *in situ* transect). Thus, the horizontal convergence of water parcels of different ages since upwelling (and thus different plankton communities) created finescale variations in the distribution of plankton abundances across the front, thus the generation of cross-frontal plankton patchiness.

The critical mechanisms underlying cross-frontal plankton patchiness have been previously discussed in other studies; however, they are often treated – and analyzed – separately. These key concepts can be summarized by the following three points: (1) a front is a mosaic of distinct water parcels brought together by convergence; (2) plankton patchiness can be explained to only a limited extent by hydrographic properties; and (3) plankton communities transform while they are advected by currents, particularly in response to nutrient injections. Below, we discuss how these ideas have been applied in previous literature and conclude that combining these concepts within a Lagrangian framework provides us with a more holistic view of physical-biological interactions at ocean fronts.

Refining our view of finescale patchiness at ocean fronts

We found that E-Front was very patchy on small spatial scales (approximately 1-5 km). The front was composed of a mosaic of water parcels contrasting in terms of biology (i.e., the plankton community), hydrography (i.e., the water-mass type derived from temperature and salinity), and history (i.e., the origin and trajectory).

Our conclusion thus extends and complements previous findings about fronts in the CCS. For instance, Mangolte et al. (2023) demonstrated the existence of sub-frontal-scale plankton patchiness at multiple fronts in the CCE, including E-Front. Furthermore, de Verneil et al. (2019), by inferring water-mass histories from finite size Lyapunov exponents, showed that water parcels with different biological and hydrographic signatures converged at E-Front. By integrating both the approaches and data presented in Mangolte et al. (2023) and de Verneil et al. (2019) for E-Front, we have shown that cross-frontal plankton community structure was well explained by upstream and along-trajectory factors.

These results challenge the traditional representation of a front as either a well-defined, localized boundary between two distinct biogeochemical provinces (Tzortzis et al., 2021; Mousing et al., 2016; Haberlin et al., 2019; Clayton et al., 2014), or as a homogeneous patch of enhanced productivity that emerges from a (typically) less productive background (Yoder et al., 1994; Franks, 1992; Allen et al., 2005; Taylor et al., 2012; Mangolte et al., 2022). These views are generally associated with a focus on the local processes that control plankton community structure: in the first view, the two provinces contain different plankton communities because of the different environmental conditions (e.g., temperature, nutrients, light, etc.), while in the second view the productive patches are explained as a response to an enhanced nutrient supply by a vertical frontal circulation or enhanced mixing (Mahadevan, 2016; Lévy et al., 2018). Instead, we emphasize the role of the horizontal circulation that brings together plankton communities with distinct origins, and influenced by earlier conditions. We were thus able to explain the observed plankton patchiness by invoking only upwelling dynamics and Lagrangian backtracking. It should be noted that the CCS contains additional sources of nutrients farther offshore, mainly generated by finescale processes (such as the frontal circulation (Li et al., 2012; Kessouri et al., 2020) or eddy pumping (Gaube et al., 2013; Chenillat et al., 2015)). However, these sources appear to have influenced plankton patchiness at E-Front to a much smaller extent than horizontal transport from the coastal upwelling zone.

A complete description of a water parcel should include its Lagrangian history

In a coastal upwelling system, ecosystem variability can often be explained by the variability in upwelling itself; this hinges on the idea that vertical transport of nutrient-rich waters at the coast stimulates primary production, which in turn fuels biomass of higher trophic levels Rykaczewski and Checkley (2008); Checkley and Barth (2009); Chavez and Messié (2009). However, the pathways through which wind-driven upwelling influences the ecosystem involve both physical (particularly, horizontal currents) and biological (growth and predation) processes that are often difficult to disentangle. In this study, we attempted to explain the underlying drivers of plankton community structure using two approaches that connected a given water parcel to wind-driven coastal upwelling.

In the first approach (applying a water-mass type association), we based the connection between biology and hydrography on the following assumption: water parcels with a CU signature were likely more recently upwelled than water parcels with a CC signature, and thus CU waters likely contained higher nutrient concentrations more recently than CC waters. However, our results showed that the assumptions underlying this first approach were too simplistic, especially at very small spatial scales. For example, recently upwelled water may have acquired a CC signature by mixing with offshore waters that had recirculated inshore. Thus, we learned that we needed to understand the Lagrangian trajectories of each individual water parcel to better analyze the relationship between their hydrographic and biological signatures.

Therefore, in the second approach, we used a Lagrangian backtracking analysis to explicitly describe the upwelling conditions experienced by a given water parcel. We found that the timing and location of upwelling influenced the biological history of each water parcel, and that qualitatively describing a water parcel as "recently upwelled" (as was the case with the first approach) was not precise enough to explain biological patterns. For example, we found that two CU water parcels may have been accurately described as "recently upwelled," but if 20 days had elapsed since upwelling for the first one and 50 days for the second, they would have had very different plankton

communities (Figure 8). The location and intensity of upwelling may have also affected the concentration and composition of nutrients available (Jacox et al., 2015, 2018). For example, dissolved iron supply, which exerts a bottom-up control on phytoplankton biomass, varies spatially along the coast, depending on factors such as shelf width, degree of sediment resuspension, and riverine inputs (Forsch et al., 2023; Hutchins et al., 1998; Till et al., 2019). These processes may drive some biological patchiness, which has been seen with diatoms across fronts (Brzezinski et al., 2015). Indeed, investigating the effects of initial nutrient concentrations and composition would require dedicated analyses that, while beyond the scope of this study, should receive further attention.

Overall, our results showed that in order to understand the drivers of plankton structure in a highly dynamic system, a local, hydrographic description of the water masses is not sufficient: all CU waters are not biologically equivalent, and sometimes CU water parcels can have more in common (in terms of biology) with a CC water parcel than another CU water parcel. The division of ocean basins into water masses, or biogeochemical provinces, is a powerful tool to understand large scale patterns of biodiversity (Irigoien et al., 2004; Longhurst, 2006; Beaugrand et al., 2019). However, at smaller spatio-temporal scales, this question is more appropriately addressed through a Lagrangian approach that describes the history of the water parcels.

The Lagrangian history: a powerful framework to understand plankton community structure

Many studies, using a variety of approaches, have investigated how plankton communities carried by horizontal currents transform in response to an initial nutrient injection, driven by coastal upwelling or by other processes. For instance, empirical studies have taken advantage of iron fertilization experiments to explore how phytoplankton blooms develop in response to a natural or artificial iron source (Abraham et al., 2000; Boyd et al., 2007; Robinson et al., 2014), while retentive eddies give a unique glimpse into the transformation of a virtually isolated plankton community over a few weeks

even months (Lehahn et al., 2011; Chenillat et al., 2015). Other studies have used growth-advection models–validated by *in situ* observations–to describe how chlorophyll and zooplankton patches are generated downstream of a nutrient source (Lehahn et al., 2017; Ser-Giacomi et al., 2023; Messié and Chavez, 2017; Messié et al., 2022).

It is worth noting that most Lagrangian studies have investigated the biological consequences of nutrient injections by applying a forward-in-time approach. Very few studies have adopted a backward-in-time approach to uncover the processes generating the observed distribution of plankton, as we did. In one of these few studies, Hernández-Carrasco et al. (2023) indeed showed that the locations of diatom blooms were best explained by Lagrangian diagnostics that integrated nutrient injections along the trajectory over the previous three months. A backward-in-time approach was also used by Chabert et al. (2021), but to understand patterns of biogeochemical processes (primary production and export) rather than ecological processes.

In this study, we applied a novel approach that built on previous work but differed from most of them in two major ways: first, it was purely empirical; second, it used a backward-in-time framework. Thus, our combined *in situ*-satellite approach allowed us to go beyond an exploration of the biological consequences of coastal upwelling and showed that Lagrangian trajectories contributed significantly to shaping the local, patchy distributions of plankton.

Conclusion

In this study, we employed a novel Lagrangian framework based on empirical data (*in situ* sampling and satellite observations) and water-parcel backtracking to demonstrate that the observed plankton patchiness across a front in the California upwelling region can be explained by distinct biological histories along converging trajectories. We found that the distribution of plankton is better explained by a metric like time since upwelling than by the hydrographic properties of the water parcel. This underscores the notion that in order to identify the processes driving frontal plankton communities, we must view them as responses to their spatial and temporal histories rather than solely result-

ing from local frontal dynamics. For instance, the many frontal studies in the CCS (including the present study and others referenced above) show that even superficially similar fronts located in the same region can be driven by completely different processes (e.g., nutrient injections by the frontal vertical circulation or horizontal transport from the coastal upwelling), and that more effort should be directed toward identifying these processes.

Thus, we encourage the widespread adoption of Lagrangian approaches such as the backtracking analysis presented here, modeling studies, or dedicated *in situ* sampling strategies aimed at collecting data along water-parcel trajectories. Such sampling strategies can include drifting arrays, which are valuable tools if they are deployed over time intervals sufficient to capture the targeted ecosystem dynamics (which may be up to a few weeks or months) (McKee et al., 2023; Kranz et al., 2020; Wang et al., 2020). Other strategies may also include ship sampling guided by real-time satellite imaging (Rousselet et al., 2019). Simultaneously measuring several physical and biogeochemical variables (including vertical currents, nutrient fluxes, growth and grazing rates, etc.) is a continuing challenge, but new technologies are developing to improve our measurements (Zheng et al., 2023). The inclusion of these Lagrangian approaches will be beneficial to research efforts aimed at gaining a better understand of the mechanisms generating and maintaining biodiversity in the ocean, especially at small scales.

Acknowledgments

The authors would like to warmly thank Peter J. S. Franks, Marina Lévy, Mark Ohman, Ralf Goericke, Pierre Chabert, Katherine Zaba, and Michael Stukel for providing data, guidance, and/or feedback. The authors are also grateful to Peter J. S. Franks (schematic) and Freya Hammar (schematic and icons) for their illustrations, and the ship/science crews on the *R/V Melville* in August 2012. SG was funded by the NSF GRFP and Scripps Institution of Oceanography. IM was funded by an ENS/Sorbonne Université PhD grant, a Fulbright scholarship, and CNES. Support for CCE LTER was provided by NSF OCE-1637632/OCE-1026607/OCE-2224726.

Data Availability

The satellite-derived data used for our analyses and/or figures can be downloaded from the CMEMS website (https://marine.copernicus.eu/) and the Aviso+ website (https://www.aviso.altimetry.fr/en/home.html). The velocity data set is cataloged here: https://doi.org/10.48670/mds-00327. The sea-surface temperature data set is cataloged here: https://doi.org/10.48670/moi-00169. The FSLE data set is cataloged here: https://doi.org/10.24400/527896/a01-2022.002. The P1208 cruise data are available on the CCE LTER Datazoo website (https://oceaninformatics.ucsd.edu/datazoo/catalogs/ccelter/datasets) or from the Environmental Data Initiative (searchable through the ezCatalog: https://ccelter.ucsd.edu/data/). The Coastal Upwelling Transport Index data are available here: https://mjacox.com/upwelling-indices/.

References

Abraham, E. R. (1998). The generation of plankton patchiness by turbulent stirring. *Nature*, 391(6667):577–580.

Abraham, E. R., Law, C. S., Boyd, P. W., Lavender, S. J., Maldonado, M. T., and Bowie, A. R. (2000). Importance of stirring in the development of an iron-fertilized phytoplankton bloom. *Nature*, 407(6805):727–730.

Allen, J. T., Brown, L., Sanders, R., Moore, C. M., Mustard, A., Fielding, S., Lucas, M., Rixen, M., Savidge, G., Henson, S., and Mayor, D. (2005). Diatom carbon export enhanced by silicate upwelling in the northeast Atlantic. *Nature*, 437(7059):728–732.

Barth, J. A., Pierce, S. D., and Smith, R. L. (2000). A separating coastal upwelling jet at Cape Blanco, Oregon and its connection to the California Current System. *Deep. Res. Part II Top. Stud. Oceanogr.*, 47(5-6):783–810.

515 Beaugrand, G., Edwards, M., and Hélaouët, P. (2019). An ecological partition of the Atlantic Ocean
516 and its adjacent seas. *Prog. Oceanogr.*, 173(July 2018):86–102.

517 Bednaršek, N. and Ohman, M. D. (2015). Changes in pteropod distributions and shell dissolution
518 across a frontal system in the California Current System. *Mar. Ecol. Prog. Ser.*, 523:93–103.

519 Bograd, S. J., Buil, M. P., Lorenzo, E. D., Castro, C. G., Schroeder, I. D., Goericke, R., Anderson,
520 C. R., Benitez-Nelson, C., and Whitney, F. A. (2015). Changes in source waters to the Southern
521 California Bight. *Deep. Res. Part II Top. Stud. Oceanogr.*, 112:42–52.

522 Bograd, S. J., Schroeder, I. D., and Jacox, M. G. (2019). A water mass history of the Southern Cali-
523 fornia current system. *Geophys. Res. Lett.*, 46(12):6690–6698.

524 Bouquet, J. M., Troedsson, C., Novac, A., Reeve, M., Lechtenbörger, A. K., Massart, W., Skaar,
525 K. S., Aasjord, A., Dupont, S., and Thompson, E. M. (2018). Increased fitness of a key appendic-
526 ularian zooplankton species under warmer, acidified seawater conditions. *PLoS One*, 13(1):1–19.

527 Bourne, H. L., Bishop, J. K., Connors, E. J., and Wood, T. J. (2021). Carbon export and fate beneath
528 a dynamic upwelled filament off the California coast. *Biogeosciences*, 18(10):3053–3086.

529 Boyd, P. W., Jickells, T., Law, C. S., Blain, S., Boyle, E. A., Buesseler, K. O., Coale, K. H., Cullen,
530 J. J., De Baar, H. J., Follows, M., Harvey, M., Lancelot, C., Levasseur, M., Owens, N. P., Pollard,
531 R., Rivkin, R. B., Sarmiento, J., Schoemann, V., Smetacek, V., Takeda, S., Tsuda, A., Turner, S.,
532 and Watson, A. J. (2007). Mesoscale iron enrichment experiments 1993-2005: Synthesis and
533 future directions. *Science (80-.).*, 315(5812):612–617.

534 Brzezinski, M. A., Krause, J. W., Bundy, R. M., Barbeau, K. A., Franks, P., Goericke, R., Landry,
535 M. R., and Stukel, M. R. (2015). Enhanced silica ballasting from iron stress sustains carbon ex-
536 port in a frontal zone within the California Current. *J. Geophys. Res. Ocean.*, 120(7):4654–4669.

Chabert, P., D'Ovidio, F., Echevin, V., Stukel, M. R., and Ohman, M. D. (2021). Cross-Shore Flow and Implications for Carbon Export in the California Current Ecosystem: A Lagrangian Analysis. *J. Geophys. Res. Ocean.*, 126(2):1–14.

Chavez, F. P. and Messié, M. (2009). A comparison of Eastern Boundary Upwelling Ecosystems. *Prog. Oceanogr.*, 83(1-4):80–96.

Checkley, D. M. and Barth, J. A. (2009). Patterns and processes in the California Current System. *Prog. Oceanogr.*, 83(1-4):49–64.

Chelton, D. B., Gaube, P., Schlax, M. G., Early, J. J., and Samelson, R. M. (2011). The influence of nonlinear mesoscale eddies on near-surface oceanic chlorophyll. *Science (80-.).*, 334(6054):328–332.

Chenillat, F., Franks, P. J., Rivière, P., Capet, X., Grima, N., and Blanke, B. (2015). Plankton dynamics in a cyclonic eddy in the Southern California Current System. *J. Geophys. Res. Ocean.*, 120(8):5566–5588.

Clayton, S., Dutkiewicz, S., Jahn, O., and Follows, M. J. (2013). Dispersal, eddies, and the diversity of marine phytoplankton. *Limnol. Oceanogr. Fluids Environ.*, 3(1):182–197.

Clayton, S., Nagai, T., and Follows, M. J. (2014). Fine scale phytoplankton community structure across the Kuroshio Front. *J. Plankton Res.*, 36(4):1017–1030.

Cohen, A. C. and Morin, J. G. (1990). Patterns of Reproduction in Ostracodes: a Review. *J. Crustac. Biol.*, 10(2):184–212.

De Verneil, A. and Franks, P. J. (2015). A pseudo-Lagrangian method for remapping ocean biogeochemical tracer data: Calculation of net Chl-a growth rates. *J. Geophys. Res. Ocean.*, 120(7):4962–4979.

559 de Verneil, A., Franks, P. J., and Ohman, M. D. (2019). Frontogenesis and the Creation of Fine-
560 Scale Vertical Phytoplankton Structure. *J. Geophys. Res. Ocean.*, 124(3):1509–1523.

561 Deibel, D. and Lowen, B. (2012). A review of the life cycles and life-history adaptations of pelagic
562 tunicates to environmental conditions. *ICES J. Mar. Sci.*, 69(3):358–369.

563 D'Ovidio, F., De Monte, S., Alvain, S., Dandonneau, Y., and Lévy, M. (2010). Fluid dynamical
564 niches of phytoplankton types. *Proc. Natl. Acad. Sci. U. S. A.*, 107(43):18366–18370.

565 D'Ovidio, F., Della Penna, A., Trull, T. W., Nencioli, F., Pujol, M. I., Rio, M. H., Park, Y. H., Cotté,
566 C., Zhou, M., and Blain, S. (2015). The biogeochemical structuring role of horizontal stirring:
567 Lagrangian perspectives on iron delivery downstream of the Kerguelen Plateau. *Biogeosciences*,
568 12(19):5567–5581.

569 Dugenne, M., Henderikx Freitas, F., Wilson, S. T., Karl, D. M., and White, A. E. (2020). Life and
570 death of Crocosphaera sp. in the Pacific Ocean: Fine scale predator–prey dynamics. *Limnol.*
571 *Oceanogr.*, 65(11):2603–2617.

572 Eiane, K. and Ohman, M. D. (2004). Stage-specific mortality of Calanus finmarchicus, Pseudo-
573 calanus elongatus and Oithona similis on Fladen Ground, North Sea, during a spring bloom. *Mar.*
574 *Ecol. Prog. Ser.*, 268(3):183–193.

575 Forsch, K. O., Fulton, K. C., Weiss, M. M., Krause, J. W., Stukel, M. R., and Barbeau, K. A. (2023).
576 Iron Limitation and Biogeochemical Effects in Southern California Current Coastal Upwelling
577 Filaments. *J. Geophys. Res. Ocean.*, 128(11):e2023JC019961.

578 Franks, P. J. S. (1992). Phytoplankton blooms at fronts: patterns, scales, and physical forcing mech-
579 anisms.

580 Gangrade, S. and Franks, P. J. (2023). Phytoplankton Patches at Oceanic Fronts Are Linked to

581 Coastal Upwelling Pulses: Observations and Implications in the California Current System. *J.*
582 *Geophys. Res. Ocean.*, 128(3):1–27.

583 Gaube, P., Chelton, D. B., Strutton, P. G., and Behrenfeld, M. J. (2013). Satellite observations of
584 chlorophyll, phytoplankton biomass, and Ekman pumping in nonlinear mesoscale eddies. *J. Geo-*
585 *phys. Res. Ocean.*, 118(12):6349–6370.

586 Goericke, R. and Montoya, J. P. (1998). Estimating the contribution of microalgal taxa to chloro-
587 phyll a in the field - Variations of pigment ratios under nutrient- and light-limited growth. *Mar.*
588 *Ecol. Prog. Ser.*, 169:97–112.

589 Gorsky, G., Ohman, M. D., Picheral, M., Gasparini, S., Stemmann, L., Romagnan, J. B., Cawood,
590 A., Pesant, S., García-Comas, C., and Prejger, F. (2010). Digital zooplankton image analysis us-
591 ing the ZooScan integrated system. *J. Plankton Res.*, 32(3):285–303.

592 Gower, J. F., Denman, K. L., and Holyer, R. J. (1980). Phytoplankton patchiness indicates the fluc-
593 tuation spectrum of mesoscale oceanic structure. *Nature*, 288(5787):157–159.

594 Haberlin, D., Raine, R., McAllen, R., and Doyle, T. K. (2019). Distinct gelatinous zooplankton
595 communities across a dynamic shelf sea. *Limnol. Oceanogr.*, 64(4):1802–1818.

596 Hernández-Carrasco, I., Rossi, V., Navarro, G., Turiel, A., Bracco, A., and Orfila, A. (2023). Flow
597 Structures With High Lagrangian Coherence Rate Promote Diatom Blooms in Oligotrophic Wa-
598 ters. *Geophys. Res. Lett.*, 50(15):1–12.

599 Hutchins, D. A., DiTullio, G. R., Zhang, Y., and Bruland, K. W. (1998). An iron limitation mosaic
600 in the California upwelling regime. *Limnol. Oceanogr.*, 43(6):1037–1054.

601 Huyer, A. (1983). Coastal upwelling in the California current system. *Prog. Oceanogr.*, 12(3):259–
602 284.

603 Huyer, A., Kosro, P. M., Fleischbein, J., Ramp, S. R., Stanton, T., Washburn, L., Chavez, F. P.,
604 Cowles, T. J., Pierce, S. D., and Smith, R. L. (1991). Currents and water masses of the Coastal
605 Transition Zone off northern California, June to August 1988. *J. Geophys. Res. Ocean.*,
606 96(C8):14809–14831.

607 Irigoien, X., Hulsman, J., and Harris, R. P. (2004). Global biodiversity patterns of marine phyto-
608 plankton and zooplankton. *Nature*, 429(6994):863–867.

609 Jacox, M. G., Bograd, S. J., Hazen, E. L., and Fiechter, J. (2015). Sensitivity of the California Cur-
610 rent nutrient supply to wind, heat, and remote ocean forcing. *Geophys. Res. Lett.*, 42(14):5950–
611 5957.

612 Jacox, M. G., Edwards, C. A., Hazen, E. L., and Bograd, S. J. (2018). Coastal Upwelling Revis-
613 ited: Ekman, Bakun, and Improved Upwelling Indices for the U.S. West Coast. *J. Geophys. Res.*
614 *Ocean.*, 123(10):7332–7350.

615 Jönsson, B. F. and Watson, J. R. (2016). The timescales of global surface-ocean connectivity. *Nat.*
616 *Commun.*, 7:1–6.

617 Kessouri, F., Bianchi, D., Renault, L., McWilliams, J. C., Frenzel, H., and Deutsch, C. A. (2020).
618 Submesoscale Currents Modulate the Seasonal Cycle of Nutrients and Productivity in the Califor-
619 nia Current System. *Global Biogeochem. Cycles*, 34(10):1–15.

620 Kosro, P. M. and Huyer, A. (1986). CTD and velocity surveys of seaward jets off northern Califor-
621 nia, July 1981 and 1982. *J. Geophys. Res. Ocean.*, 91(C6):7680–7690.

622 Kotori, M. (1999). Life cycle and growth rate of the chaetognath parasagitta elegans in the northern
623 North Pacific Ocean. *Plankt. Biol. Ecol.*, 46(2):153–158.

624 Kranz, S. A., Wang, S., Kelly, T. B., Stukel, M. R., Goericke, R., Landry, M. R., and Cassar, N.
625 (2020). Lagrangian Studies of Marine Production: A Multimethod Assessment of Productivity

626 Relationships in the California Current Ecosystem Upwelling Region. *J. Geophys. Res. Ocean.*,
627 125(6).

628 Lehahn, Y., D'Ovidio, F., and Koren, I. (2018). A satellite-based Lagrangian view on phytoplankton
629 dynamics. *Ann. Rev. Mar. Sci.*, 10(September):99–119.

630 Lehahn, Y., D'Ovidio, F., Lévy, M., Amitai, Y., and Heifetz, E. (2011). Long range transport of a
631 quasi isolated chlorophyll patch by an Agulhas ring. *Geophys. Res. Lett.*, 38(16):1–6.

632 Lehahn, Y., Koren, I., Sharoni, S., D'Ovidio, F., Vardi, A., and Boss, E. (2017). Dispersion/dilution
633 enhances phytoplankton blooms in low-nutrient waters. *Nat. Commun.*, 8:1–8.

634 Levin, S. A. and Segel, L. A. (1976). Hypothesis for origin of planktonic patchiness.

635 Lévy, M., Franks, P. J., and Smith, K. S. (2018). The role of submesoscale currents in structuring
636 marine ecosystems. *Nat. Commun.*, 9(1):4758.

637 Lévy, M., Jahn, O., Dutkiewicz, S., and Follows, M. J. (2014). Phytoplankton diversity and commu-
638 nity structure affected by oceanic dispersal and mesoscale turbulence. *Limnol. Oceanogr. Fluids*
639 *Environ.*, 4(1):67–84.

640 Lewandowska, A. M., Striebel, M., Feudel, U., Hillebrand, H., and Sommer, U. (2015). The impor-
641 tance of phytoplankton trait variability in spring bloom formation. *ICES J. Mar. Sci.*, 72(6):1908–
642 1915.

643 Li, Q. P., Franks, P. J., Ohman, M. D., and Landry, M. R. (2012). Enhanced nitrate fluxes and bi-
644 ological processes at a frontal zone in the southern California current system. *J. Plankton Res.*,
645 34(9):790–801.

646 Longhurst, A. R. (2006). *Ecological Geography of the Sea, Second Edition*. Elsevier.

Lynn, R. J. and Simpson, J. J. (1987). The California Current system: The seasonal variability of its physical characteristics. *J. Geophys. Res. Ocean.*, 92(C12):12947–12966.

Mahadevan, A. (2016). The Impact of Submesoscale Physics on Primary Productivity of Plankton. *Ann. Rev. Mar. Sci.*, 8(1):161–184.

Mangolte, I., Lévy, M., Dutkiewicz, S., Clayton, S., and Jahn, O. (2022). Plankton community response to fronts: winners and losers. *J. Plankton Res.*, 44(2):241–258.

Mangolte, I., Lévy, M., Haëck, C., and Ohman, M. D. (2023). Sub-frontal niches of plankton communities driven by transport and trophic interactions at ocean fronts. *Biogeosciences*, 20(15):3273–3299.

Martin, A. (2003). Phytoplankton patchiness: the role of lateral stirring and mixing. *Prog. Oceanogr.*, 57(2):125–174.

Mauzole, Y. L., Torres, H. S., and Fu, L. L. (2020). Patterns and Dynamics of SST Fronts in the California Current System. *J. Geophys. Res. Ocean.*, 125(2).

McGillicuddy, D. J. and Franks, P. J. (2019). Models of Plankton Patchiness. In *Encycl. Ocean Sci. Third Ed. Vol. 1-5*, volume 1-5, pages V5–536–V5–546. Elsevier.

McKee, D. C., Doney, S. C., Della Penna, A., Boss, E. S., Gaube, P., and Behrenfeld, M. J. (2023). Biophysical Dynamics at Ocean Fronts Revealed by Bio-Argo Floats. *J. Geophys. Res. Ocean.*, 128(3).

McWilliams, J. C. (2016). Submesoscale currents in the ocean. *Proc. R. Soc. A Math. Phys. Eng. Sci.*, 472(2189):20160117.

Messié, M. and Chavez, F. P. (2017). Nutrient supply, surface currents, and plankton dynamics predict zooplankton hotspots in coastal upwelling systems. *Geophys. Res. Lett.*, 44(17):8979–8986.

669 Messié, M., Sancho-Gallegos, D. A., Fiechter, J., Santora, J. A., and Chavez, F. P. (2022). Satellite-
670 Based Lagrangian Model Reveals How Upwelling and Oceanic Circulation Shape Krill Hotspots
671 in the California Current System. *Front. Mar. Sci.*, 9(May):1–19.

672 Messié, M., Sherlock, R. E., Huffard, C. L., Pennington, J. T., Choy, C. A., Michisaki, R. P., Gomes,
673 K., Chavez, F. P., Robison, B. H., and Smith, K. L. (2023). Coastal upwelling drives ecosys-
674 tem temporal variability from the surface to the abyssal seafloor. *Proc. Natl. Acad. Sci. U. S. A.*,
675 120(13):2017.

676 Mousing, E. A., Richardson, K., Bendtsen, J., Cetinić, I., and Perry, M. J. (2016). Evidence of
677 small-scale spatial structuring of phytoplankton alpha- and beta-diversity in the open ocean. *J.*
678 *Ecol.*, 104(6):1682–1695.

679 Ohman, M. D., Powell, J. R., Picheral, M., and Jensen, D. W. (2012). Mesozooplankton and particu-
680 late matter responses to a deep-water frontal system in the southern California Current System. *J.*
681 *Plankton Res.*, 34(9):815–827.

682 Plattner, G. K., Gruber, N., Frenzel, H., and McWilliams, J. C. (2005). Decoupling marine export
683 production from new production. *Geophys. Res. Lett.*, 32(11):1–4.

684 Renault, L., McWilliams, J. C., Kessouri, F., Jousse, A., Frenzel, H., Chen, R., and Deutsch, C.
685 (2021). Evaluation of high-resolution atmospheric and oceanic simulations of the California Cur-
686 rent System. *Prog. Oceanogr.*, 195(March):102564.

687 Rio, M. H., Mulet, S., and Picot, N. (2014). Beyond GOCE for the ocean circulation estimate: Syn-
688 ergetic use of altimetry, gravimetry, and in situ data provides new insight into geostrophic and
689 Ekman currents. *Geophys. Res. Lett.*, 41(24):8918–8925.

690 Robinson, J., Popova, E. E., Yool, A., Srokosz, M., Lampitt, R. S., and Blundell, J. R. (2014). How

691 deep is deep enough? Ocean iron fertilization and carbon sequestration in the Southern Ocean.
692 *Geophys. Res. Lett.*, 41(7):2489–2495.

693 Rossi, V., Ser-Giacomi, E., Lõpez, C., and Hernández-García, E. (2014). Hydrodynamic provinces
694 and oceanic connectivity from a transport network help designing marine reserves. *Geophys. Res.*
695 *Lett.*, 41(8):2883–2891.

696 Rousselet, L., Doglioli, A. M., de Verneil, A., Pietri, A., Della Penna, A., Berline, L., Marrec, P.,
697 Grégori, G., Thyssen, M., Carlotti, F., Barrillon, S., Simon-Bot, F., Bonal, M., D'Ovidio, F., and
698 Petrenko, A. (2019). Vertical Motions and Their Effects on a Biogeochemical Tracer in a Cy-
699 clonic Structure Finely Observed in the Ligurian Sea. *J. Geophys. Res. Ocean.*, 124(6):3561–
700 3574.

701 Rykaczewski, R. R. and Checkley, D. M. (2008). Influence of ocean winds on the pelagic ecosystem
702 in upwelling regions. *Proc. Natl. Acad. Sci. U. S. A.*, 105(6):1965–1970.

703 Sarthou, G., Timmermans, K. R., Blain, S., and Tréguer, P. (2005). Growth physiology and fate of
704 diatoms in the ocean: A review. *J. Sea Res.*, 53(1-2 SPEC. ISS.):25–42.

705 Schmid, M. S., Sponaugle, S., Thompson, A. W., Sutherland, K. R., and Cowen, R. K. (2023).
706 Drivers of plankton community structure in intermittent and continuous coastal upwelling sys-
707 tems–from microbes and microscale in-situ imaging to large scale patterns. *Front. Mar. Sci.*,
708 10(November):1–22.

709 Ser-Giacomi, E., Martinez-Garcia, R., Dutkiewicz, S., and Follows, M. J. (2023). A Lagrangian
710 model for drifting ecosystems reveals heterogeneity-driven enhancement of marine plankton
711 blooms. *Nat. Commun.*, 14(1):6092.

712 Stukel, M. R., Aluwihare, L. I., Barbeau, K. A., Chekalyuk, A. M., Goericke, R., Miller, A. J.,
713 Ohman, M. D., Ruacho, A., Song, H., Stephens, B. M., and Landry, M. R. (2017). Mesoscale

ocean fronts enhance carbon export due to gravitational sinking and subduction. *Proc. Natl. Acad. Sci. U. S. A.*, 114(6):1252–1257.

Stukel, M. R., Ohman, M. D., Benitez-Nelson, C. R., and Landry, M. R. (2013). Contributions of mesozooplankton to vertical carbon export in a coastal upwelling system. *Mar. Ecol. Prog. Ser.*, 491:47–65.

Taylor, A. G., Goericke, R., Landry, M. R., Selph, K. E., Wick, D. A., and Roadman, M. J. (2012). Sharp gradients in phytoplankton community structure across a frontal zone in the California Current Ecosystem. *J. Plankton Res.*, 34(9):778–789.

Till, C. P., Solomon, J. R., Cohen, N. R., Lampe, R. H., Marchetti, A., Coale, T. H., and Bruland, K. W. (2019). The iron limitation mosaic in the California Current System: Factors governing Fe availability in the shelf/near-shelf region. *Limnol. Oceanogr.*, 64(1):109–123.

Tzortzis, R., Doglioli, A. M., Barrillon, S., Petrenko, A. A., D'Ovidio, F., Izard, L., Thyssen, M., Pascual, A., Barceló-Llull, B., Cyr, F., Tedetti, M., Bhairy, N., Garreau, P., Dumas, F., and Gregori, G. (2021). Impact of moderately energetic fine-scale dynamics on the phytoplankton community structure in the western Mediterranean Sea. *Biogeosciences*, 18(24):6455–6477.

Wang, S., Kranz, S. A., Kelly, T. B., Song, H., Stukel, M. R., and Cassar, N. (2020). Lagrangian Studies of Net Community Production: The Effect of Diel and Multiday Nonsteady State Factors and Vertical Fluxes on O2/Ar in a Dynamic Upwelling Region. *J. Geophys. Res. Biogeosciences*, 125(6):1–19.

Wilkins, D., Van Sebille, E., Rintoul, S. R., Lauro, F. M., and Cavicchioli, R. (2013). Advection shapes Southern Ocean microbial assemblages independent of distance and environment effects. *Nat. Commun.*, 4(May).

Yoder, J. A., Ackleson, S. G., Barber, R. T., Flament, P., and Balch, W. M. (1994). A line in the sea. *Nature*, 371(6499):689–692.

Zaba, K. D., Franks, P. J., and Ohman, M. D. (2021). The California Undercurrent as a Source of Upwelled Waters in a Coastal Filament. *J. Geophys. Res. Ocean.*, 126(2).

Zaba, K. D., Rudnick, D. L., Cornuelle, B. D., Gopalakrishnan, G., and Mazloff, M. R. (2018). Annual and interannual variability in the California current system: Comparison of an ocean state estimate with a network of underwater gliders. *J. Phys. Oceanogr.*, 48(12):2965–2988.

Zheng, B., Lucas, A. J., Franks, P. J., Schlosser, T. L., Anderson, C. R., Send, U., Davis, K., Barton, A. D., and Sosik, H. M. (2023). Dinoflagellate vertical migration fuels an intense red tide. *Proc. Natl. Acad. Sci. U. S. A.*, 120(36):2017.

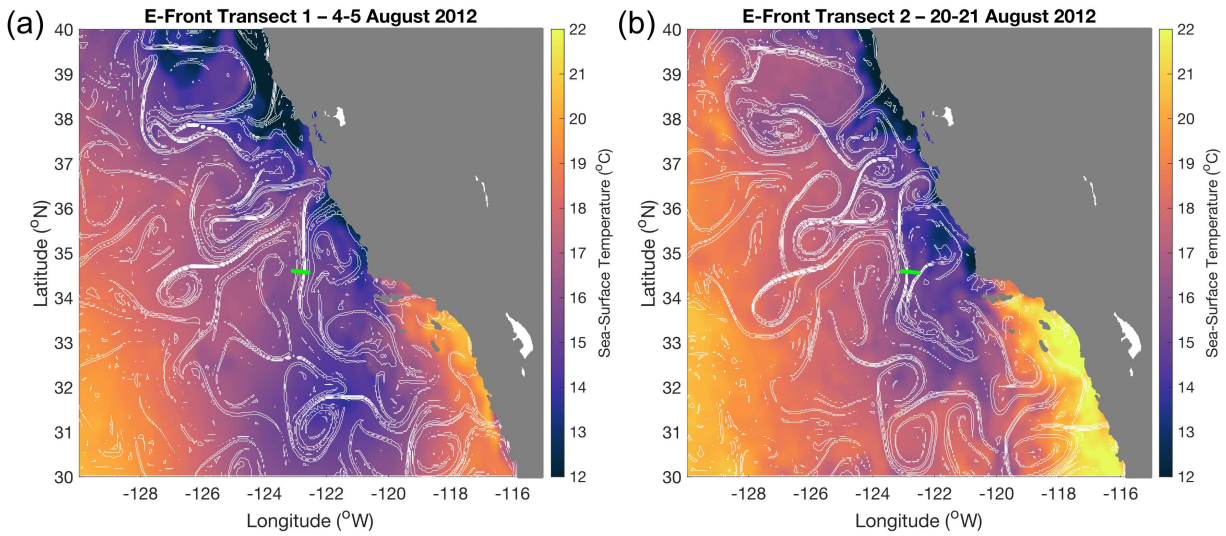

Figure 1: Maps of sea-surface temperature (SST in $^{\circ}C$, color scale) and finite size Lyapunov exponents (FSLEs in d^{-1}, white contours) averaged over the duration of E-Front Transect E1 (a), and Transect E2 (b). FSLE contours represent values from to $0\ d^{-1}$ to $-0.3\ d^{-1}$, in increments of $0.1\ d^{-1}$. Green markers indicate the locations of the sampling stations in each transect. Filaments of recently upwelled cold water were advected offshore via mesoscale stirring features (outlined by the FSLE contours) at various locations along the coast (e.g., at 38°N in Transect E2).

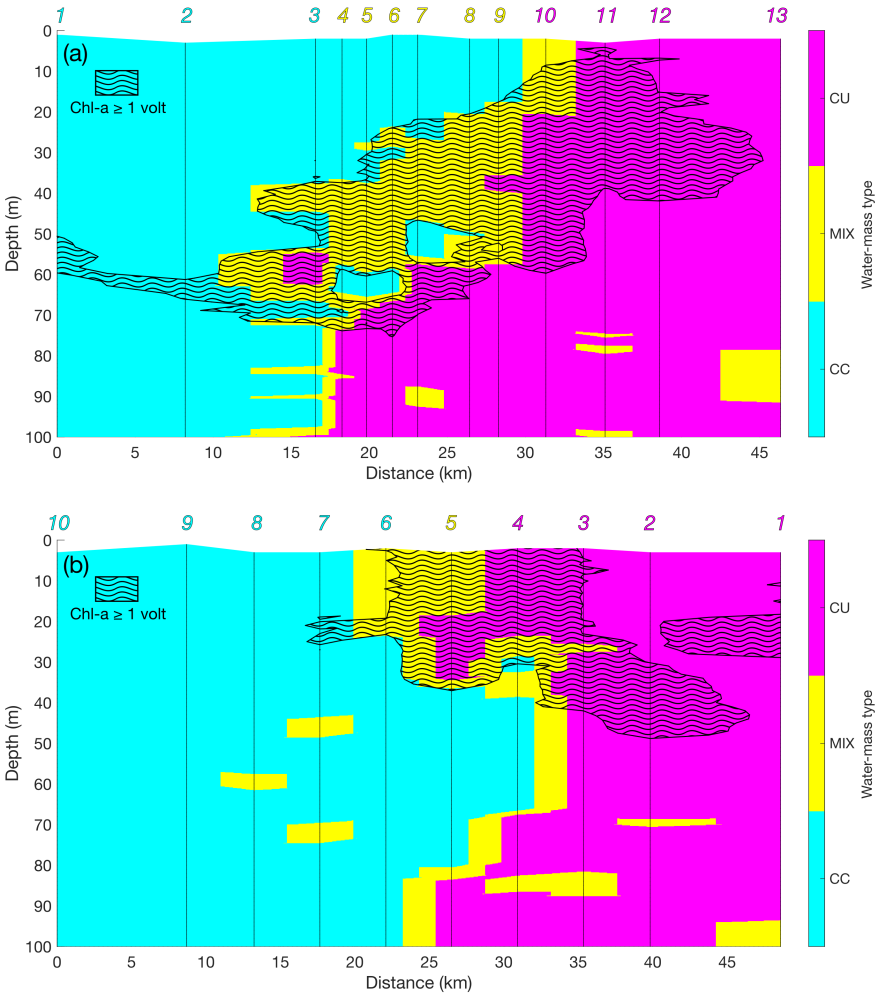

Figure 2: Vertical sections (0-100 m) across the front from west (offshore, on the left) to east (inshore, on the right) of water masses for Transect E1 (a) and Transect E2 (b). Cyan, magenta, and yellow colors indicate California Current (CC), California Undercurrent (CU), and Mixed (MIX) waters, respectively. Here, the frontal interface coincided with the MIX waters (yellow). Hatches show the position of chlorophyll-*a* patches (fluorescence $\geq 1\ V$). Vertical black lines indicate the position of the CTD stations, with the station number colored by the majority water-mass type on the top x-axis.

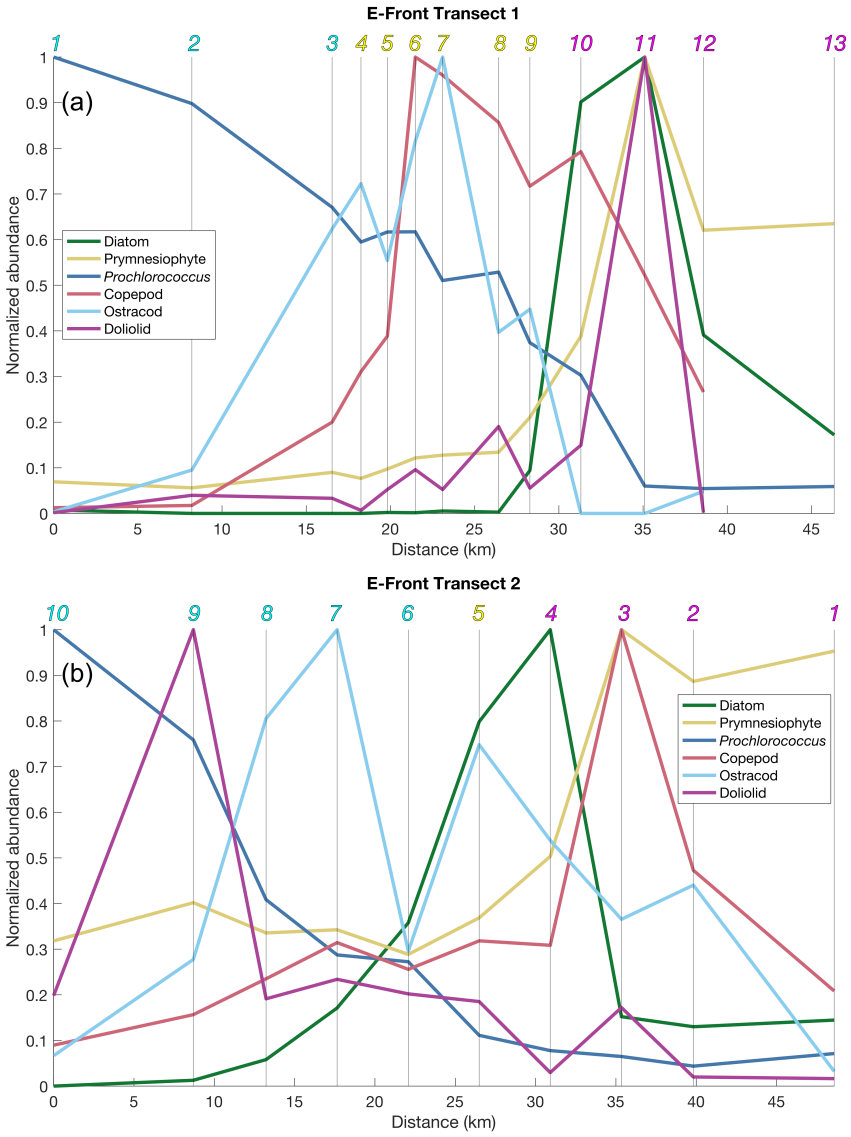

Figure 3: Cross-frontal abundances, normalized by the maximum abundance for each taxon in each transect, of select bacteria, phytoplankton, and zooplankton taxa in Transect E1 (a) and Transect E2 (b). Top x-axis and vertical black lines indicate locations of the stations for each transect, and coloring of transect station numbers correspond to water-mass type as defined in Figure 2 (cyan for CC, magenta for CU, and yellow for MIX). The color of each plotted line represents a specific taxon.

Table 1: Association between plankton taxa and water-mass types. Different market indicate different associations: X = statistically significant association; x = minor association; - = no association. The upper rows (Chlorophytes to *Prochlorococcus*) indicate taxa that were consistently associated with a single water-mass type (CC or CU), while the bottom rows (Chlorophyll-*a* fluorescence to Other crustaceans) indicate taxa that were not consistently associated with a single water-mass type. The full results of the Kruskal-Wallis tests are provided in Supporting Information Table S2 and Table S3.

Taxa	CC		MIX		CU	
	E1	E2	E1	E2	E1	E2
Chlorophytes	-	-	-	-	X	X
Cryptophytes	-	-	-	-	X	X
Dinoflagellates	-	-	-	-	X	x
Pelagophytes	-	-	-	-	X	x
Prymnnesiophytes	-	-	-	-	X	x
Heterotrophic bacteria	-	-	-	-	X	X
Rhizaria	-	-	-	-	x	X
Pteropods	-	-	-	-	X	X
Prochlorococcus	X	X	-	-	-	-
Chlorophyll-*a* fluorescence (0-100 m)	-	-	X	X	-	-
Ostracods	-	-	x	x	-	-
Diatoms	-	-	-	x	-	-
Synechococcus	-	-	X	-	-	-
Pico-eukaryotes	-	-	X	-	-	-
Appendicularians	-	-	x	-	-	-
Chaetognaths	-	-	x	-	-	-
Cnidarians	-	-	x	-	-	-
Doliolids	-	X	-	-	x	-
Copepods (Calanoids, Oithona, Others)	-	-	x	-	-	x
Polychaetes	-	-	X	-	-	x
Euphausiids	-	-	x	-	-	x
Other crustaceans	-	-	x	-	-	x

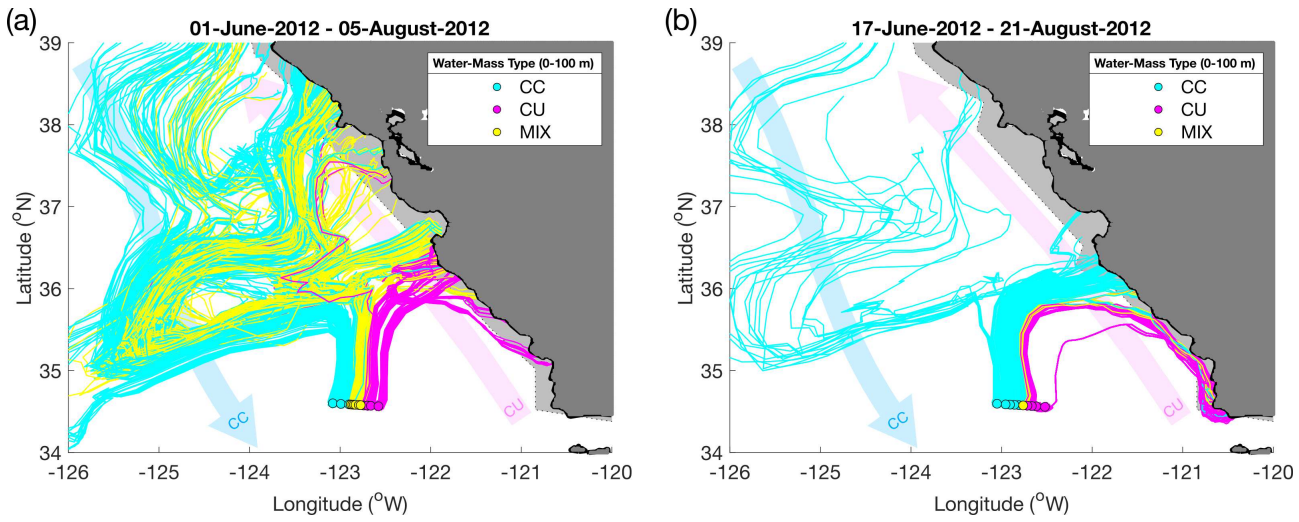

Figure 4: Trajectories of water parcels sampled across E-Front Transect E1 (a) and Transect E2 (b) in the two months before sampling. Trajectories were computed from backward-in-time advection, using a velocity field that includes a geostrophic and a 15-m depth Ekman component. Filled circles show the locations of the sampled stations, with each station consisting of a CTD cast and a Bongo net tow. For each station, the back-trajectories of 100 points, randomly seeded in a 5-km radius around the actual station, were computed. The colors of each circle and trajectory pathline correspond to the dominant water-mass type of the water parcel when it was sampled (as defined in Figure 1). The light gray region outlined by the dotted line indicates the coastal upwelling region, which encompasses the coastal region within approximately 25 km of the coastline. The blue and magenta arrows show the approximate position and direction of the CC and CU, respectively.

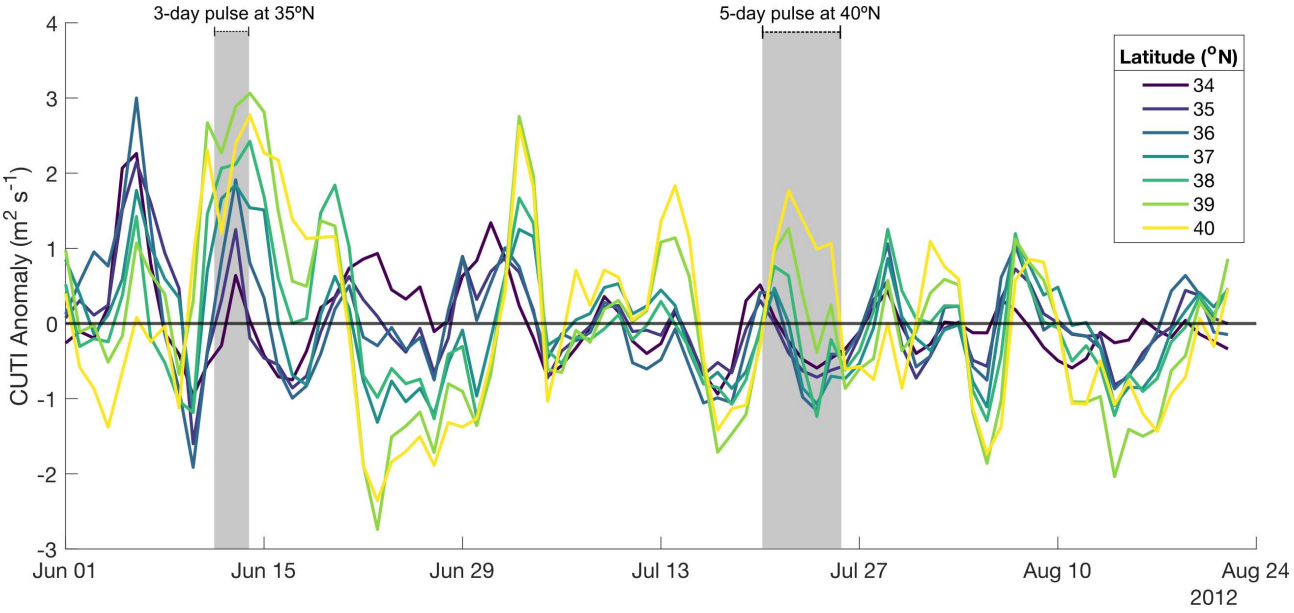

781 Figure 5: Times series of the Coastal Upwelling Transport Index (CUTI) anomaly from 1 June to
782 24 August 2012 for different latitudinal bands (colors) in the California Current System. Two con-
783 trasting upwelling pulses are highlighted (gray shaded regions), illustrating upwelling variability in
784 terms of location, timing, duration, and intensity.

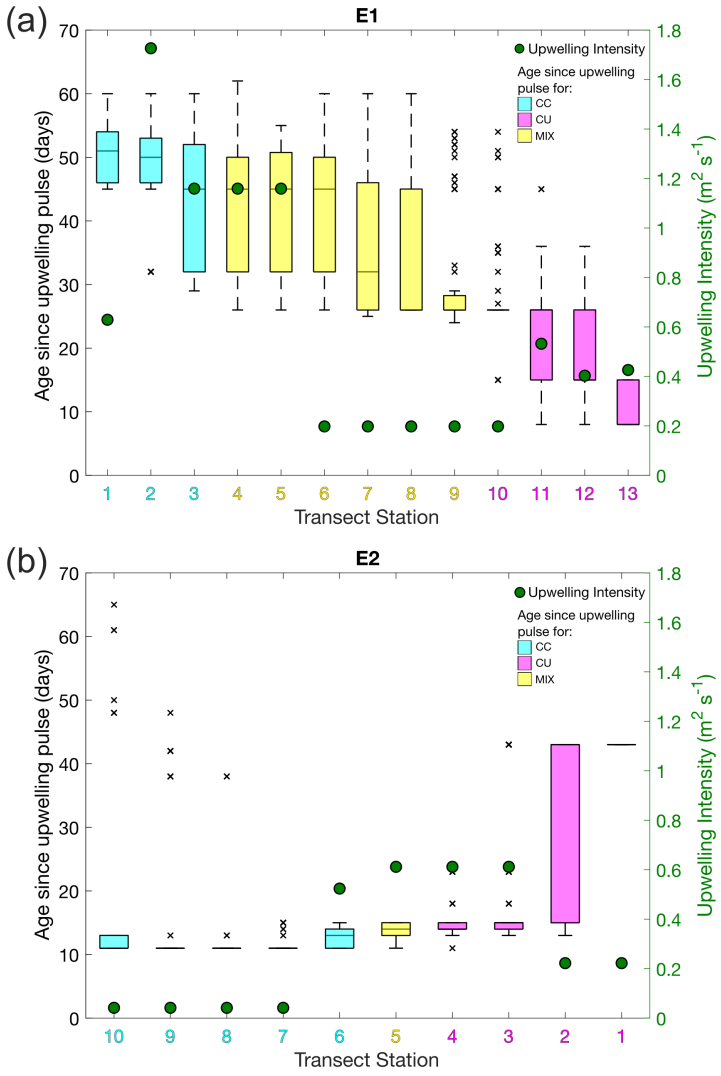

Figure 6: Upwelling conditions experienced by the ensemble of trajectories for each sampled station of Transect E1 (a) and Transect E2 (b). Box plots show the interquartile range of age since upwelling pulse in days (left y-axis, with outliers indicated by black x-markers). Box plots and transect station numbers are colored by the majority water-mass type at each station. Green filled circles indicate the median upwelling intensity, calculated as the CUTI anomaly, when parcels were at the coast (right y-axis in green).

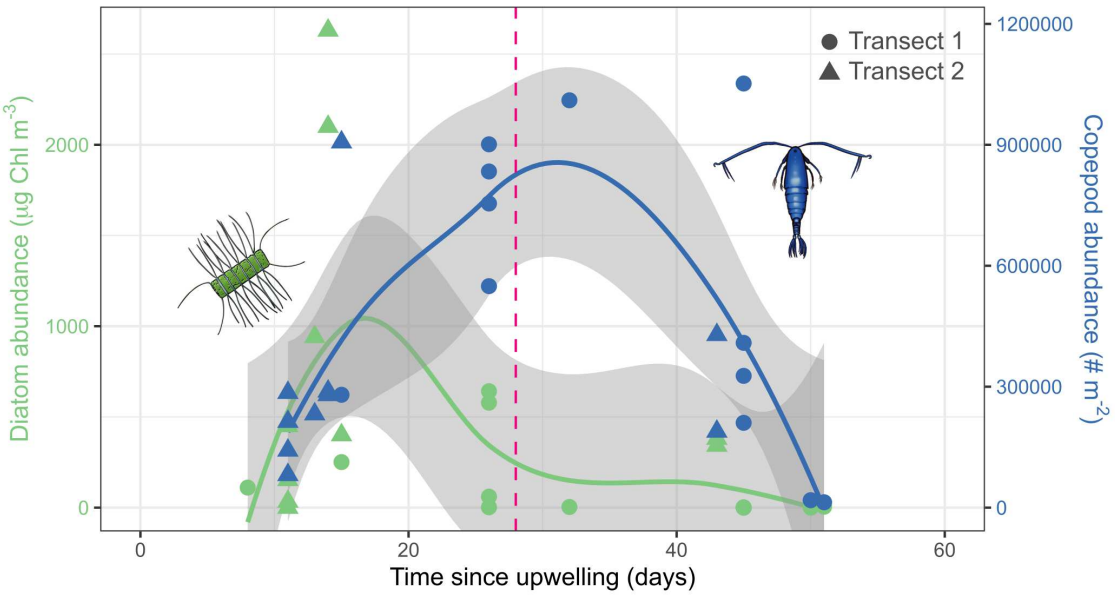

Figure 7: Relationship between plankton abundance and time since upwelling for diatoms (prey) in green and copepods (predator) in blue. Each marker represents one station (triangles for Transect E1, circles for Transect E2). The green and blue lines represent the lowess fits (f=0.75) for the diatom and copepod abundances respectively. The gray shaded regions indicate the 95% confidence interval for each lowess fit. The vertical dashed line in magenta indicates the typical copepod generation time (28 days). Plankton illustrations: Freya Hammar.

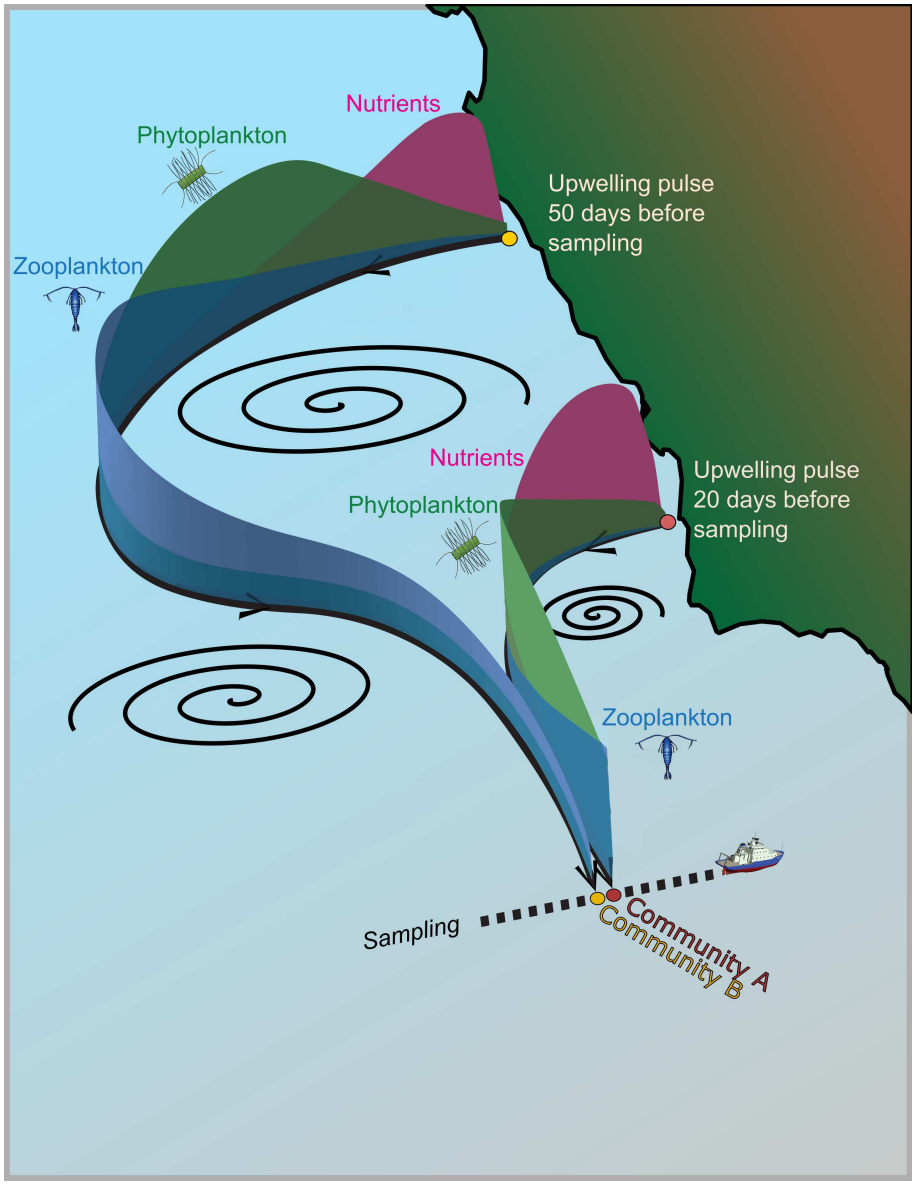

Figure 8: Schematic representation of the biological transformation taking place in upwelled water parcels and their subsequent convergence at a front. The longer trajectory (left) originates in the north during an upwelling pulse that occurs 50 days before sampling, and the shorter trajectory (right) originates in the south during an upwelling pulse that occurs 20 days before sampling. Along each trajectory, nutrients, phytoplankton, and zooplankton concentrations peak in succession, resulting in two very different communities sampled during the cross-frontal transect. Illustration: Peter J.S. Franks and Freya Hammar. Icons: Freya Hammar (plankton) and Woods Hole Oceanographic Institution (ship).

Supporting Information for:

Patchiness of plankton communities at fronts explained by Lagrangian history of upwelled water parcels

Shailja Gangrade[1*] and Inès Mangolte[2,3]

[1]Scripps Institution of Oceanography, University of California San Diego, La Jolla, California, USA

[2]LOCEAN (Laboratoire d'Océanographie et du Climat), Institut Pierre Simon Laplace (Sorbonne Université/CNRS/IRD/MNHN), Paris, France

[3]ENTROPIE, IRD/Université de la Réunion/Université de Nouvelle-Calédonie/CNRS/Ifremer, Noumea, New Caledonia

[*]Corresponding author: Shailja Gangrade, sgangrad@ucsd.edu

Biological responses of non-diatom and non-copepod taxa

The diatom-copepod food chain, despite its importance (both in terms of quantity and in ecological and biogeochemical consequences), is one dimension of a very complex plankton ecosystem. On the one hand, many other grazing zooplankton taxa also consume diatoms (particularly filter-feeding tunicates); on the other hand, the diet of copepods can include a variety of sources including other phytoplankton, zooplankton, or detritus (Whitmore and Ohman, 2021).

Many factors might explain why the collected data only showed a significant biological response for diatoms and copepods. In the case of non-diatom phytoplankton (Figure S6), it is possible that a bloom developed at the subsurface only and was thus not measured in our surface measurements. Or, it is also possible that – unlike diatoms – the other phytoplankton taxa were unable to escape grazing pressure due to their slower growth rates (Inomura et al., 2023). In the case of carnivorous zooplankton (Figure S7), it is likely that the duration of our backtracking analysis (two months) was too short relative to their reproduction rates. We would expect large changes in their abundances to be visible after several months or even years. For instance, Messié et al. (2023) described a "damping effect" in the California upwelling region by which metazoan organisms with longer lifespans or those located deeper in the water column (i.e., mesopelagic or benthic) respond slower to environmental forcings than phytoplankton or micro-zooplankton: the response time scales may be months to years as opposed to days to weeks.

Moreover, some taxa showed multiple peaks in abundance within water parcels of different ages, which could indicate more complex trophic interactions. For instance, appendicularians (Figure S8a) showed an initial peak at about 10 days, consistent with their fast growth rate in response to the diatom bloom (Capitanio and Esnal, 1998), followed by a second peak at about 30 days, which could be generated by the consumption of copepod fecal pellets.

The only taxon other than diatoms and copepods that showed a clear relationship with age since upwelling pulse was rhizarians. The abundance of rhizarians peaked at approximately 30 days (Figure S8b). While the feeding strategies and growth rates of rhizarian organisms are extremely diverse (Biard, 2015; Biard and Ohman, 2020), the time scale of this increase in abundance is consistent with a growth response to an increase in the availability of their nutrition source (whether they are photosynthetic, eat inorganic nutrients, diatoms, or detritus).

Table S1. List of plankton taxa sampled during the E-Front transects, the methodologies used (sampling and identification methods), and the vertical resolution.

Sample	Instrument	Taxa included	Depth
Niskin bottle	Flow Cytometry	Heterotrophic bacteria, *Prochlorococcus* (PRO), *Synechococcus* (SYN), pico-eukaryotes	Discrete levels 0-120 m
Niskin bottle	HPLC	Diatoms, dinoflagellates, coccolithophores, pelagophytes, chlorophytes, cryptophytes	Surface
Bongo net	ZooScan	3 copepod groups (calanoids, oithonoids, and others), pteropods, euphausiids, other crustaceans, rhizarians, doliolids, appendicularians, salps, pyrosomes, cnidarians+ctenophores, polychaetes, chaetognaths, ostracods	Vertically averaged 0-100 m

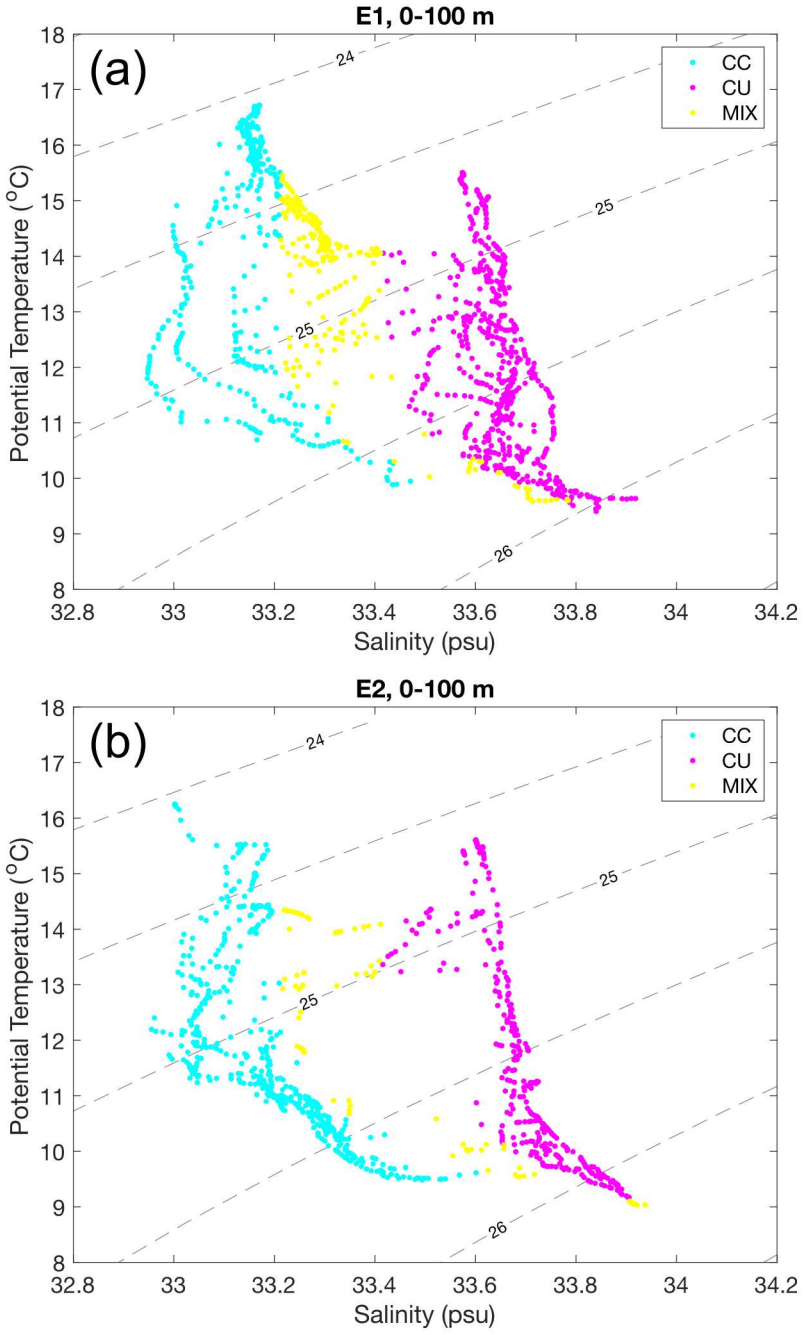

Figure S1. Salinity-temperature plots for E-Front Transect E1 (a) and Transect E2 (b) from CTD vertical profiles (0-100 m). Dashed gray lines indicate the density (σ_θ) isolines. Points are colored according to their water-mass type classification: California Current (CC, cyan), California Undercurrent (CU, magenta) and MIX (yellow).

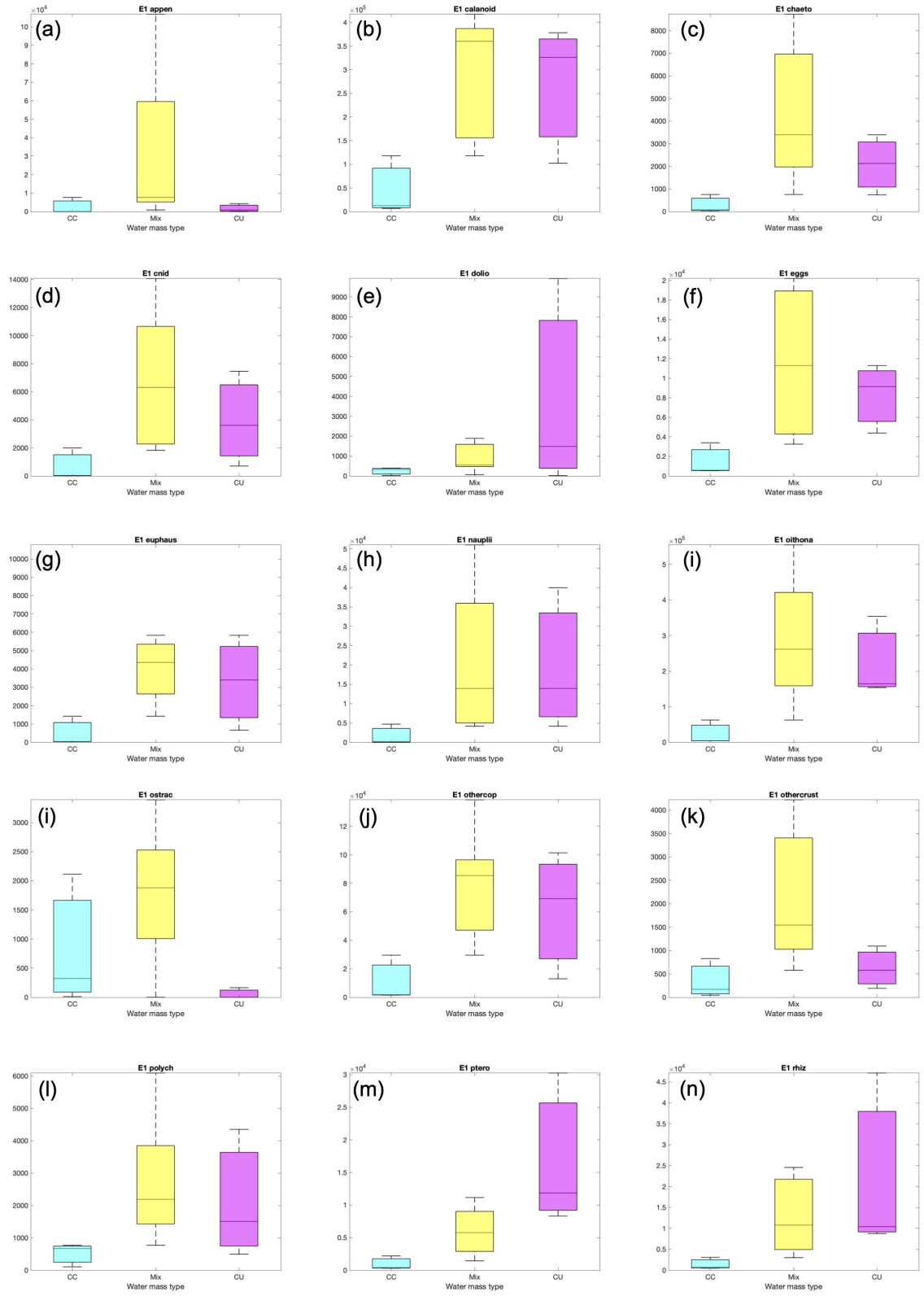

Figure S2. Distribution of zooplankton abundance ($no./m^2$) in each majority water-mass type for E-front Transect E1. Box plots indicate the median and interquartile ranges of abundance and are colored by the corresponding water-mass type (cyan for CC, yellow for MIX, and magenta for CU). Zooplankton abundances were vertically integrated (0-100m), and the majority water-mass type in the vertical water-column profile was used (see Data and Methods).

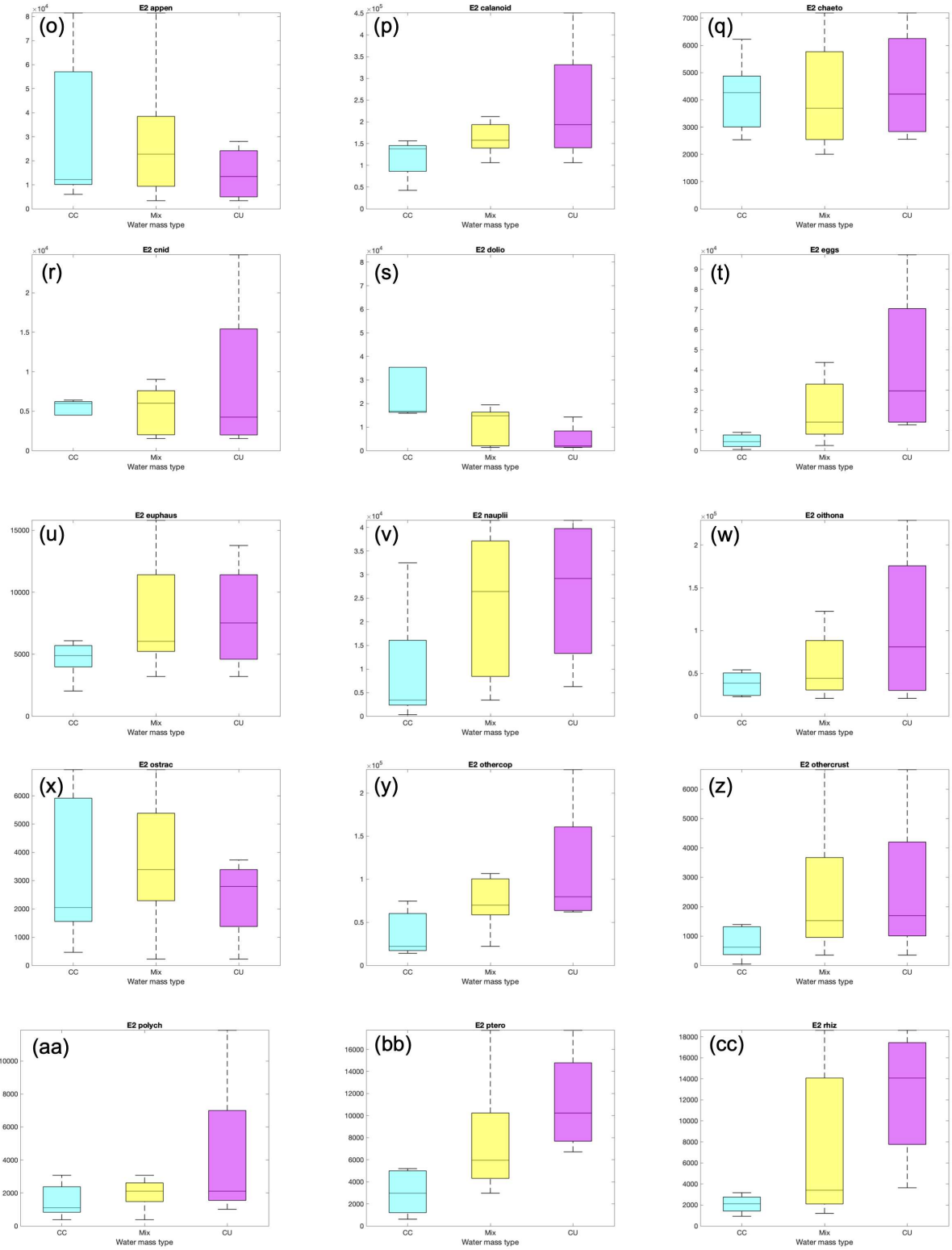

Figure S3. Same as Figure S2 above, but for E-Front Transect E2.

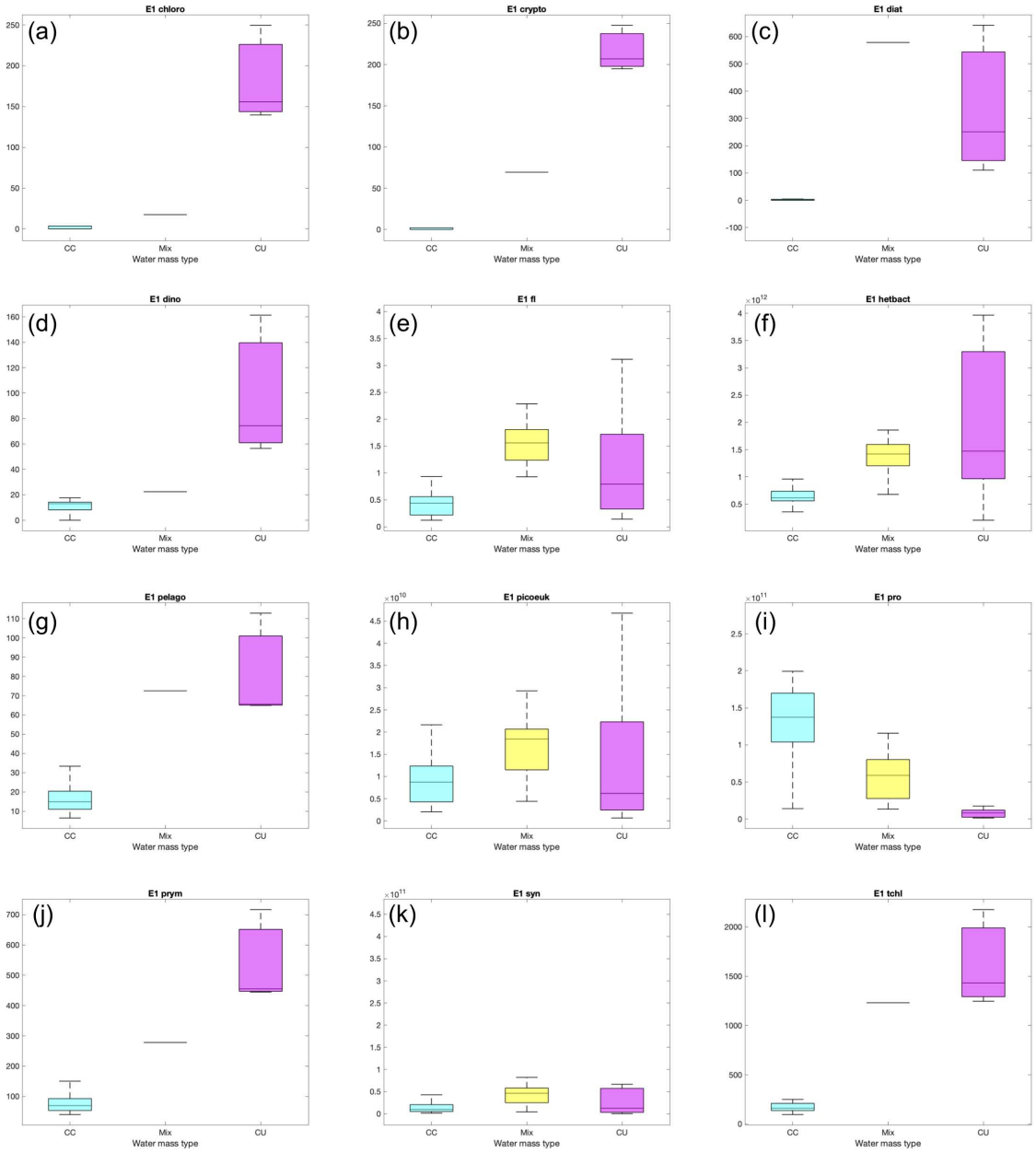

Figure S4. Distribution of picoplankton and phytoplankton abundance in each majority water-mass type for E-Front Transect E1. Box plots indicate the median and interquartile ranges of abundance and are colored by corresponding water-mass type (cyan for CC, yellow for MIX, and magenta for CU). Picoplankton abundance (*Prochlorococcus*, *Synechococcus*, picoeukaryotes, and heterotrophic bacteria, in $cells/L$) were measured with flow cytometry at each vertical level. Phytoplankton ($\mu gChl/m^3$) were measured with HPLC for the surface sample only. The water-mass types were taken at the vertical level corresponding to each sample.

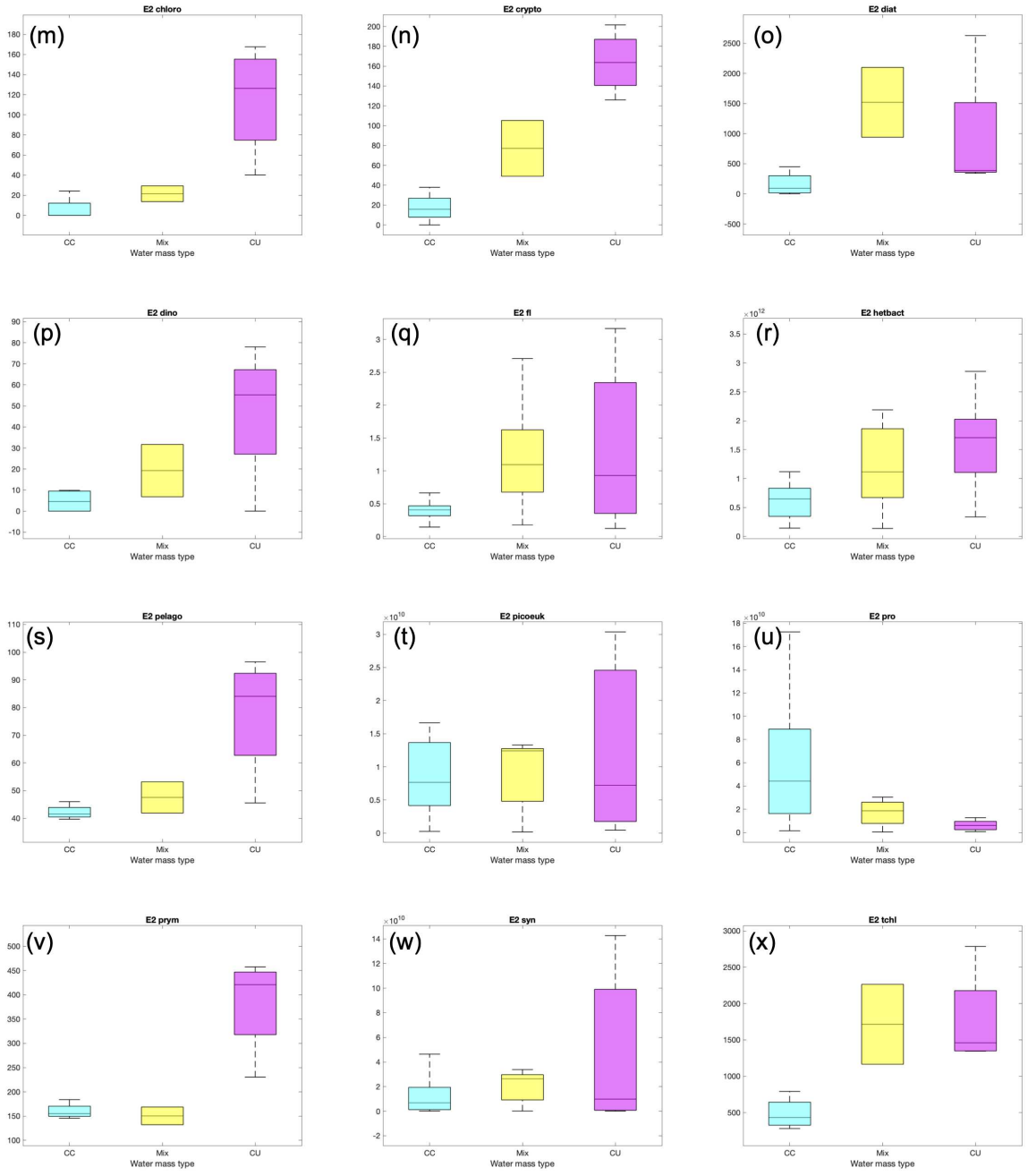

Figure S5. Same as Figure S4 above, but for E-Front Transect E2.

Table S2. Results from Kruskal-Wallis statistical tests comparing the distributions of plankton abundances in pairs of water-mass types (CC vs. CU, CC vs. MIX and CC vs. MIX) for E-Front Transect E1. High p-values (> 0.05) indicate that the distributions are not statistically different (i.e., the null hypothesis – that the data originate from the same distributions – is not rejected). In contrast, low p-values ≤ 0.01 (orange) and $0.01 < p$-value < 0.05 (yellow) indicate that the distributions are statistically different (null hypothesis is rejected).

Taxon/Group	CC vs. MIX	CC vs. CU	MIX vs. CU
chloro	0.558	0.0109	0.7485
crypto	0.3817	0.0095	0.8791
diat	0.1996	0.0377	0.9878
dino	0.4415	0.019	0.8965
fl	0	0.005	0.0111
hetbact	0	0	0.9098
pelago	0.2032	0.0391	0.988
picoeuk	0.0254	0.9393	0.0095
pro	0.01	0	0.0001
prym	0.4425	0.0192	0.8967
syn	0.0029	0.8109	0.0138
tchl	0.4425	0.0192	0.8967
appen	0.1775	0.9715	0.0989
calanoid	0.0329	0.3312	0.7239
chaeto	0.0268	0.4321	0.5359
cnid	0.0487	0.3800	0.7465
dolio	0.1981	0.2860	0.9906
eggs	0.0401	0.2448	0.8867
euphaus	0.0401	0.2448	0.8867
nauplii	0.0704	0.2077	0.9906
oithona	0.0268	0.2077	0.8692
ostrac	0.8389	0.4818	0.1181
othercop	0.0401	0.2448	0.8867
othercrust	0.0364	0.8228	0.1912
polych	0.0487	0.3800	0.7465
ptero	0.1267	0.0145	0.3025
pyro	NaN	NaN	NaN
rhiz	0.0643	0.0984	0.9576
salp	NaN	NaN	NaN
totvintfl	0.3267	0.4779	0.9953
totvintdiat	0.3267	0.4779	0.9953

Table S3. Same as Table S2 above, but for E-Front Transect E2.

Taxon/Group	CC vs. MIX	CC vs. CU	MIX vs. CU
chloro	0.6601	0.0180	0.3668
crypto	0.4869	0.0140	0.4869
diat	0.1116	0.3402	0.6667
dino	0.7777	0.2227	0.7777
fl	0.0224	0.0050	0.8300
hetbact	0.0841	0.0000	0.4874
pelago	0.6064	0.0510	0.6064
picoeuk	0.9666	0.9662	0.9963
pro	0.1458	0.0000	0.1926
prym	0.9559	0.0680	0.0903
syn	0.6079	0.7643	0.8802
tchl	0.1991	0.0378	0.9559
appen	0.9976	0.7389	0.6575
calanoid	0.1935	0.1193	0.8475
chaeto	0.9710	0.9615	0.8677
cnid	0.9995	0.9827	0.9729
dolio	0.1446	0.0175	0.4306
eggs	0.0940	0.0227	0.6060
euphaus	0.2725	0.4010	0.9998
nauplii	0.1781	0.1394	0.9047
oithona	0.8621	0.7300	0.9365
ostrac	0.9024	0.9326	0.7082
othercop	0.1228	0.0918	0.8868
othercrust	0.2308	0.2327	0.9623
polych	0.7775	0.7389	0.9818
ptero	0.1446	0.0175	0.4306
pyro	NaN	NaN	NaN
rhiz	0.2725	0.0290	0.3621
salp	NaN	NaN	NaN
totvintfl	0.0585	0.0290	0.7810
totvintdiat	0.0585	0.0290	0.7810

Table S4. Description of water-parcel origins for each E-Front transect station based on an ensemble of back-trajectories (100 parcels seeded randomly in a 5-km radius around each station). A water parcel was considered to have originated from the coast (6th column) if its trajectory location was within 25 km of the coastline at any point during the 2-month backtracking. A water parcel was assumed to have been upwelled (last column) if it was at the coast during an upwelling pulse (positive CUTI anomaly). The median age since upwelling and pulse intensity were computed only for upwelled water parcels.

Transect	Station	Median age since upwelling (days)	Median CUTI (m^2/s)	Median CUTI anomaly (m^2/s)	Fraction of parcels from coast	Fraction of upwelled parcels
1	1	51	1.618	0.629	0.68	0.68
1	2	50	2.787	1.727	0.80	0.80
1	3	45	2.130	1.159	0.95	0.95
1	4	45	2.130	1.159	0.91	0.91
1	5	45	2.130	1.159	0.92	0.91
1	6	45	1.020	0.198	0.94	0.94
1	7	32	1.020	0.198	0.95	0.95
1	8	26	1.020	0.198	0.92	0.92
1	9	26	1.020	0.198	0.95	0.95
1	10	26	1.020	0.198	1	1
1	11	26	1.503	0.532	1	1
1	12	15	1.225	0.403	1	0.96
1	13	8	1.248	0.426	1	0.89
2	1	43	0.909	0.222	1	1
2	2	43	0.909	0.222	1	1
2	3	15	1.433	0.612	1	1
2	4	14	1.433	0.612	1	1
2	5	14	1.433	0.612	1	1
2	6	13	1.345	0.524	1	1
2	7	11	0.863	0.042	1	1
2	8	11	0.863	0.042	1	1
2	9	11	0.863	0.042	1	0.91
2	10	11	0.863	0.042	0.96	0.91

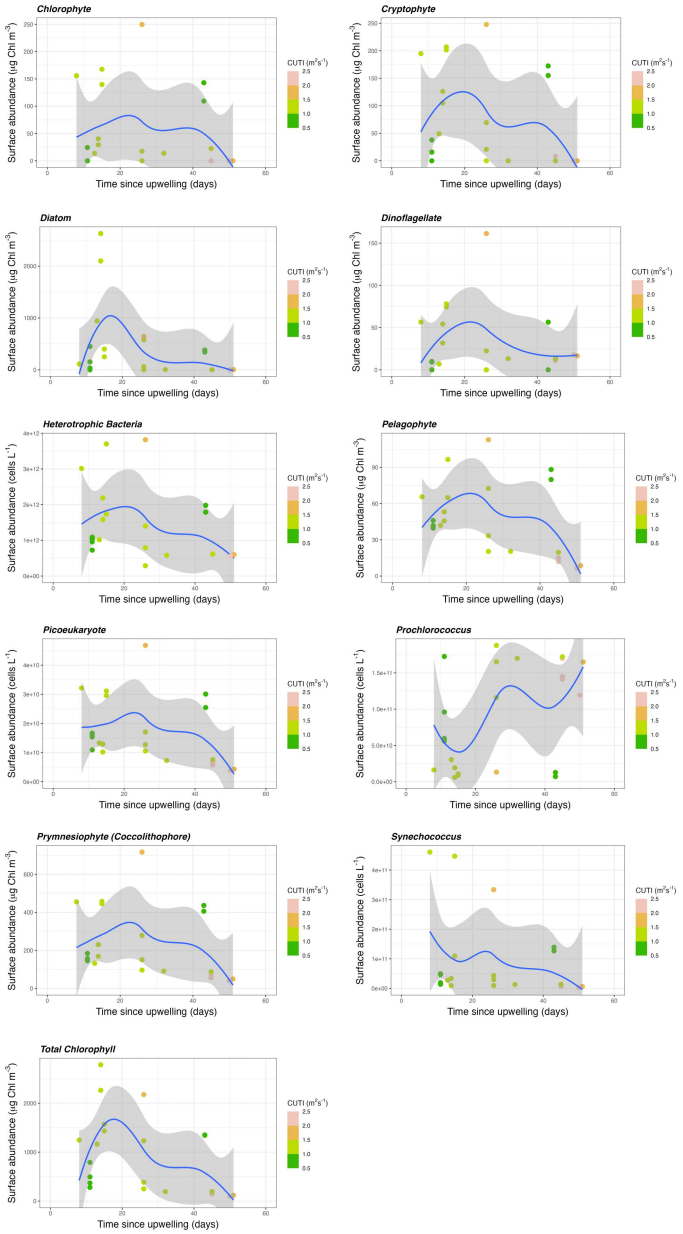

Figure S6. Relationship between phytoplankton and bacteria abundance and age (time) since upwelling, in days. Each marker represents one station; the points include data from both transects. Blue lines represent the lowess fits (f=0.75) of time vs. abundance, with gray shaded regions indicating the 95% confidence interval. The color of the points indicate the median upwelling pulse intensity calculated from the magnitude of CUTI when parcels were at the coast.

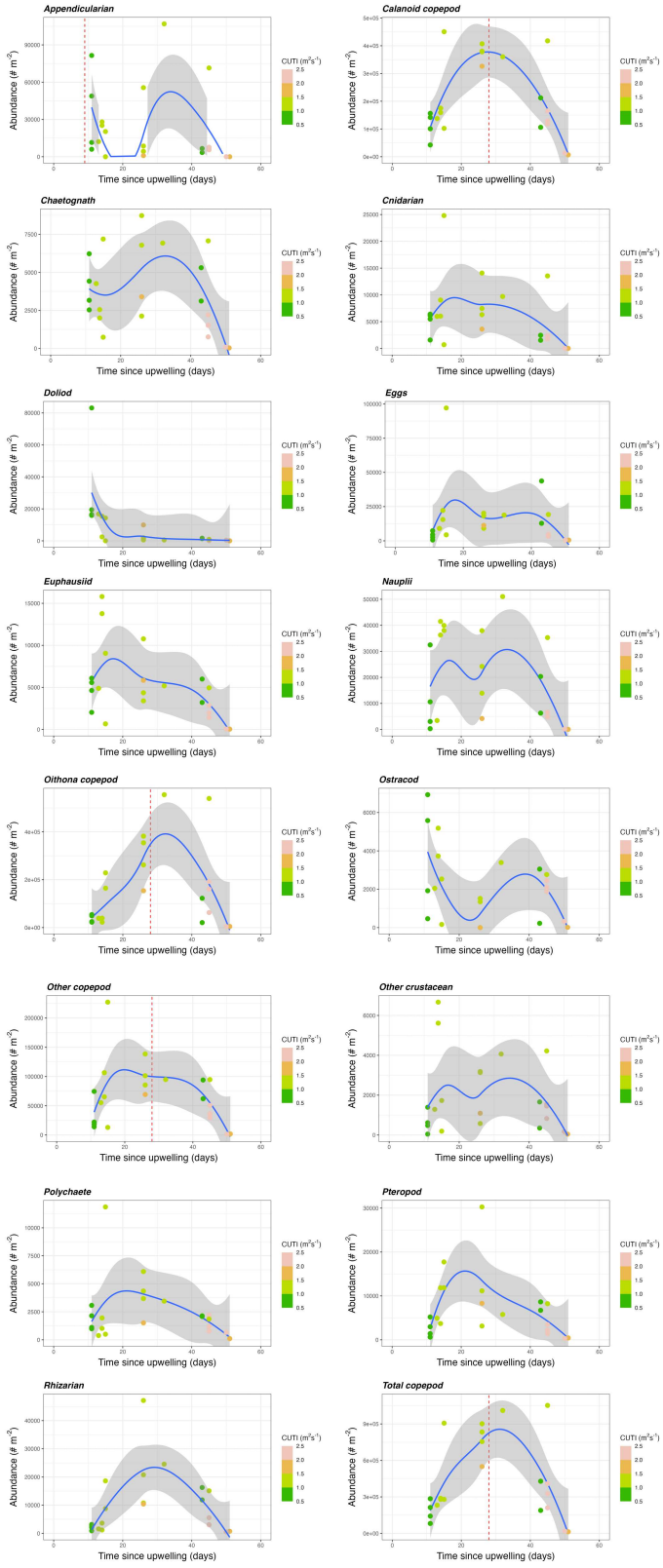

Figure S7. Relationship between zooplankton (and related taxa) abundances and age (time) since upwelling. Each marker represents one station; the points include data from both transects. Blue lines represent the lowess fits (f=0.75) of time vs. abundance, with gray shaded regions indicating the 95% confidence interval. The color of the points indicate the median upwelling pulse intensity calculated from the magnitude of CUTI when parcels were at the coast. Vertical dashed lines in red, when plotted, indicate the estimated generation time of the taxon (e.g., 28 days for copepods).

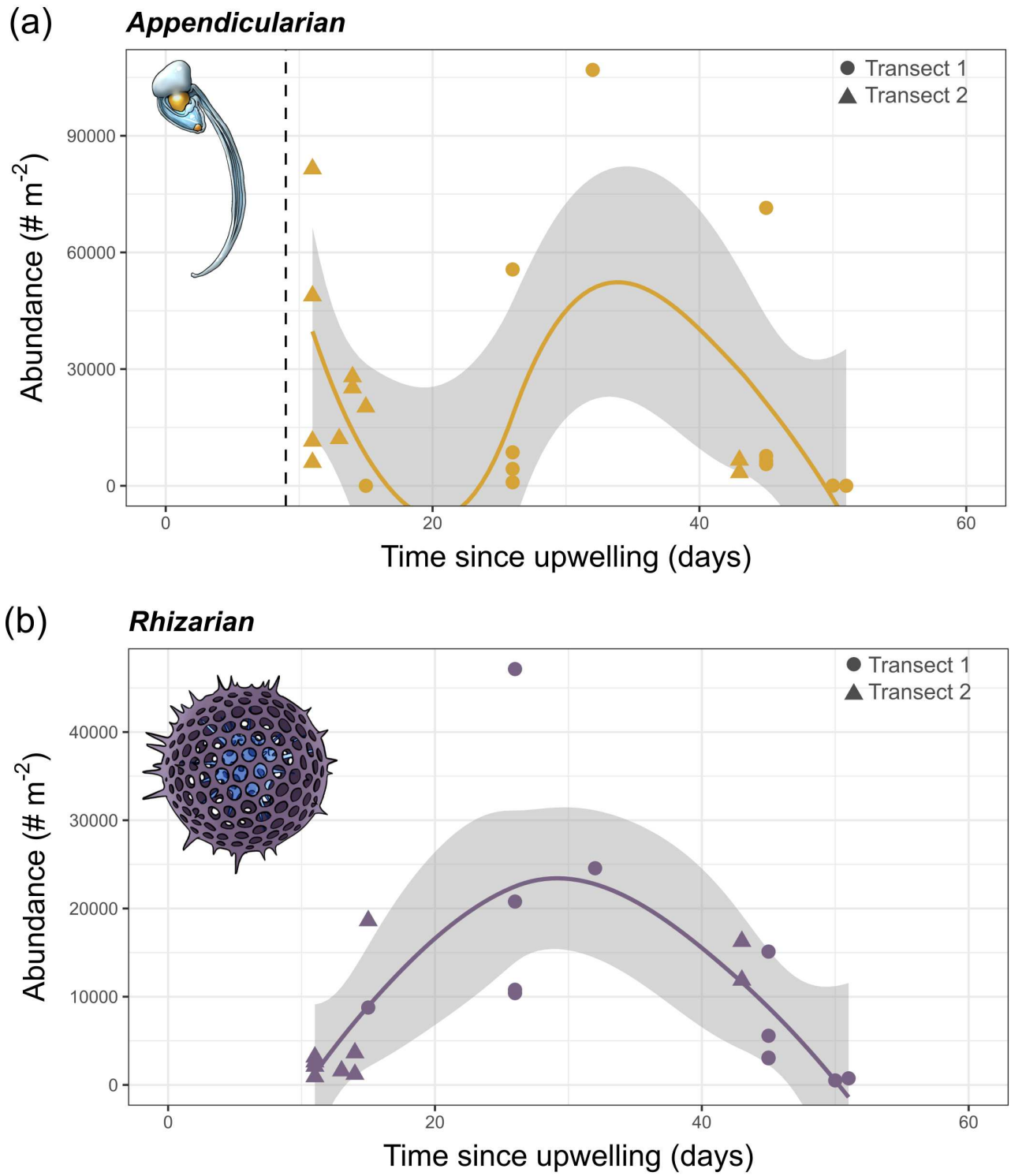

Figure S8. Relationship between plankton abundance and age (time) since upwelling for (a) appendicularians and (b) rhizarians. Each marker represents one station (triangles for Transect E1, circles for Transect E2). The orange and purple lines represent the lowess fits (f=0.75) of time vs. abundance for appendicularians and rhizarians respectively. Gray shaded regions indicate the 95% confidence interval of the lowess fits. The vertical dashed line in (a) shows the typical appendicularian generation time (9 days). Plankton illustrations: Freya Hammar.

References

Biard, M. T. (2015). *Diversité, biogéographie et écologie des Collodaires (Radiolaires) dans l'océan mondial*. PhD thesis.

Biard, T. and Ohman, M. D. (2020). Vertical niche definition of test-bearing protists (Rhizaria) into the twilight zone revealed by in situ imaging. *Limnol. Oceanogr.*, 65(11):2583–2602.

Capitanio, F. L. and Esnal, G. B. (1998). Vertical distribution of maturity stages of Oikopleura dioica (tunicata, appendicularia) in the frontal system off Valdes Peninsula, Argentina. *Bulletin of Marine Science*, 63(3):531–539.

Inomura, K., Karlusich, J. J. P., Dutkiewicz, S., Deutsch, C., Harrison, P. J., and Bowler, C. (2023). High growth rate of diatoms explained by reduced carbon requirement and low energy cost of silica deposition. *Microbiology Spectrum*, 11(3):e03311–22.

Messié, M., Sherlock, R. E., Huffard, C. L., Pennington, J. T., Choy, C. A., Michisaki, R. P., Gomes, K., Chavez, F. P., Robison, B. H., and Smith, K. L. (2023). Coastal upwelling drives ecosystem temporal variability from the surface to the abyssal seafloor. *Proc. Natl. Acad. Sci. U. S. A.*, 120(13):2017.

Whitmore, B. M. and Ohman, M. D. (2021). Zooglider-measured association of zooplankton with the fine-scale vertical prey field. *Limnol. Oceanogr.*, 66(10):3811–3827.

Supplementary Files

This is a list of supplementary files associated with this preprint. Click to download.

- GangradeMangolteLO9April2024submitedSupportingInformation.pdf